Title

Black manganese-rich crusts on a Gothic cathedral

Authors

Macholdt, Dorothea S
Herrmann, Siegfried
Jochum, Klaus Peter
et al.

Publication Date

2017-12-01

DOI

10.1016/j.atmosenv.2017.10.022

Atmospheric Environment 171 (2017) 205–220

Contents lists available at ScienceDirect

Atmospheric Environment

journal homepage: www.elsevier.com/locate/atmosenv

Black manganese-rich crusts on a Gothic cathedral

Dorothea S. Macholdt[a,b,*], Siegfried Herrmann[b], Klaus Peter Jochum[b], A.L.David Kilcoyne[c], Thomas Laubscher[d], Jonas H.K. Pfisterer[e], Christopher Pöhlker[a], Beate Schwager[b], Bettina Weber[f], Markus Weigand[g], Katrin F. Domke[e], Meinrat O. Andreae[a,h]

[a] Biogeochemistry Department, Max Planck Institute for Chemistry, Mainz, Germany
[b] Climate Geochemistry Department, Max Planck Institute for Chemistry, Mainz, Germany
[c] Lawrence Berkeley National Laboratory, Berkeley, CA, United States
[d] Freiburger Münster Münsterbauverein, Freiburg, Germany
[e] Molecular Spectroscopy Department, Max Planck Institute for Polymer Research, Mainz, Germany
[f] Multiphase Chemistry Department, Max Planck Institute for Chemistry, Mainz, Germany
[g] Modern Magnetic Systems Department, Max Planck Institute for Intelligent Systems, Stuttgart, Germany
[h] Geology and Geophysics Department, King Saud University, Riyadh, Saudi Arabia

ARTICLE INFO

Keywords:
Manganese crusts
Portable XRF
Freiburger münster
Rock varnish
Vehicle emission
Manganese deposition mechanisms

ABSTRACT

Black manganese-rich crusts are found worldwide on the façades of historical buildings. In this study, they were studied exemplarily on the façade of the Freiburger Münster (Freiburg Minster), Germany, and measured in-situ by portable X-ray fluorescence (XRF). The XRF was calibrated to allow the conversion from apparent mass fractions to Mn surface density (Mn mass per area), to compensate for the fact that portable XRF mass fraction measurements from thin layers violate the assumption of a homogeneous measurement volume. Additionally, 200-nm femtosecond laser ablation-inductively coupled plasma-mass spectrometry (fs LA-ICP-MS) measurements, scanning transmission X-ray microscopy-near edge X-ray absorption fine structure spectroscopy (STXM-NEXAFS), Raman spectroscopy, and imaging by light microscopy were conducted to obtain further insight into the crust material, such as potential biogenic contributions, element distributions, trace element compositions, and organic functional groups.

While black crusts of various types are present at many places on the minster's facade, crusts rich in Mn (with a Mn surface density > 150 μg cm^{-2}) are restricted to a maximum height of about 7 m. The only exceptions are those developed on the Renaissance-Vorhalle (Renaissance Portico) at a height of about 8 m. This part of the façade had been cleaned and treated with a silicon resin as recently as 2003. These crusts thus accumulated over a period of only 12 years. Yet, they are exceptionally Mn-rich with a surface density of 1200 μg cm^{-2}, and therefore require an accumulation rate of about 100 μg cm^{-2} Mn per year.

Trace element analyses support the theory that vehicle emissions are responsible for most of the Mn supply. Lead, barium, and zinc correlate with manganese, indicating that tire material, brake pads, and resuspended road dust are likely to be the element sources. Microscopic investigations show no organisms on or in the Mn-rich crusts. In contrast, Mn-free black crusts sampled at greater heights (> 8 m) exhibited fungal and cyanobacterial encrustation. Carbon-rich spots were found by STXM-NEXAFS underneath one of the Mn-rich crusts. However, these carbon occurrences originate from soot and polycyclic aromatic hydrocarbons (PAHs) deposited on top of the crust, rather than from organisms responsible for the crust's formation, as shown by STXM-NEXAFS and Raman spectroscopic measurements. Our results suggest that the crusts develop abiogenically, with vehicle emissions as dominant element sources.

1. Introduction

Historic buildings and monuments in urban areas often show extensive dark or black discolorations, which affect their aesthetic appeal and whose restoration can have considerable economic implications (Newby et al., 1991). Until recently, most of these blackened areas were thought to be formed by the accumulation of soot, which on carbonate building materials is often incorporated into a matrix of gypsum. The main source of the soot can be traced back to fossil fuel combustion, which depending on the time and place concerned may be dominated

* Corresponding author. Biogeochemistry Department, Max Planck Institute for Chemistry, Mainz, Germany.
E-mail address: d.macholdt@mpic.de (D.S. Macholdt).

http://dx.doi.org/10.1016/j.atmosenv.2017.10.022
Received 21 April 2017; Received in revised form 6 October 2017; Accepted 9 October 2017
Available online 14 October 2017
1352-2310/

by coal burning, diesel engines, and other activities (Bonazza et al., 2005, 2007a; Brimblecombe and Grossi, 2009; De Oliveira et al., 2011; Grossi and Brimblecombe, 2002, 2008; Pio et al., 1998; Ruffolo et al., 2015; Sáiz-Jiménez and Hermosin, 2004).

The gypsum layer develops as a result of the sulfur dioxide (SO_2) released in the course of fossil fuel combustion, which can either react directly with the carbonate material or after its oxidation to sulfuric acid in the atmosphere (Bonazza et al., 2005; Brimblecombe and Grossi, 2009; Grossi and Brimblecombe, 2002; Ruffolo et al., 2015). Colored organic compounds incorporated into the coatings can result in brownish or yellowish discolorations (Bonazza et al., 2007a; Brimblecombe and Grossi, 2009; Grossi and Brimblecombe, 2008). More recently, the growth of cyanobacteria (Bonazza et al., 2007b; Uchida et al., 2016), bacteria (Miller et al., 2012), and fungi (De Oliveira et al., 2011; Gorbushina et al., 1993; Saiz-Jimenez et al., 2012; Viles and Gorbushina, 2003) was also implicated in the discoloration of exposed stone materials.

However, in the last few years it was discovered that some black crusts on buildings in urban open areas are actually Mn-rich coatings (Grissom et al., 2014; Grüner et al., 2011; Livingston et al., 2016; Uchida et al., 2016; Vicenzi et al., 2016) with an as yet unknown genesis. These black crusts lack identifiable biogenic structures (Grissom et al., 2014; Livingston et al., 2016; Vicenzi et al., 2016) and are thus dissimilar to Mn-rich crusts found in cave environments, which had often been found to be of biogenic origin (Frierdich et al., 2011; Miller et al., 2012; Saiz-Jimenez et al., 2012; White et al., 2009). Manganese-rich coatings on facades of buildings of historical interest are often present on siliceous stones, such as quartz-based sandstones, in contrast to the soot-rich crusts on limestones, marbles, or calcareous sandstones (Bonazza et al., 2005, 2007a; Brimblecombe and Grossi, 2009; Grossi and Brimblecombe, 2002, 2008). Grossi and Brimblecombe (2002) report that quartz-based sandstones behave differently from limestones and marbles, since they are resistant to sulfur-based acids in the air and they “tend to become dirtier in rain-washed areas than in sheltered areas”.

Such Mn-rich coatings were described from the Freiburger Münster, Freiburg, Germany (Fig. 1) by Grüner et al. (2011). They had also been observed on several other buildings of historical interest, such as at the church in Stödtlen, Germany (Grüner et al., 2011), the Smithsonian Institute in Washington D.C., USA (Grissom et al., 2014; Livingston et al., 2016; Vicenzi et al., 2016), and the Khmer temples in Cambodia (Uchida et al., 2016), indicating the worldwide abundance of these crusts. Manganese-rich crusts on historical buildings are not only found on sandstone building blocks, but also on laterites and bricks (Uchida et al., 2016). No systematic association has been observed between the surface roughness of the building blocks and crust development, neither on the Freiburger Münster, nor on the Smithsonian Castle (Vicenzi et al., 2016). Furthermore, the patches are most abundant on the building blocks themselves, and only to a lesser extent on the mortar between them. The crusts seem to start growing on the sandstone and only cover the mortar in cases when the crusts span several blocks, an observation also made at the Smithsonian Institute (Vicenzi et al., 2016).

As these patches disfigure the appearance of the buildings, attempts were sometimes made to seal and protect the building blocks by painting them with various coatings or sealants. At the Freiburger Münster manganese-rich crusts had been found especially prominently on the Renaissance-Vorhalle built in 1620. This addition to the minster was treated with a hydrophobic, diffusion-open silicon resin paint during restoration work in 2003 (Grüner et al., 2011), which ironically might have created conditions particularly suitable for Mn-crust growth. Another part of the minster, the Schöpfungsportal (creation portal), was treated with a pore-closing silicic acid ester on several areas. Black crusts grew at these locations within only about four years. The Schöpfungsportal is of specific interest because of existing photographic documentation spanning the last 100 years. It appears that the applied coatings have actually facilitated the growth of the black crusts, hence it is of importance to understand their genesis and formation mechanisms before considering further restoration measures.

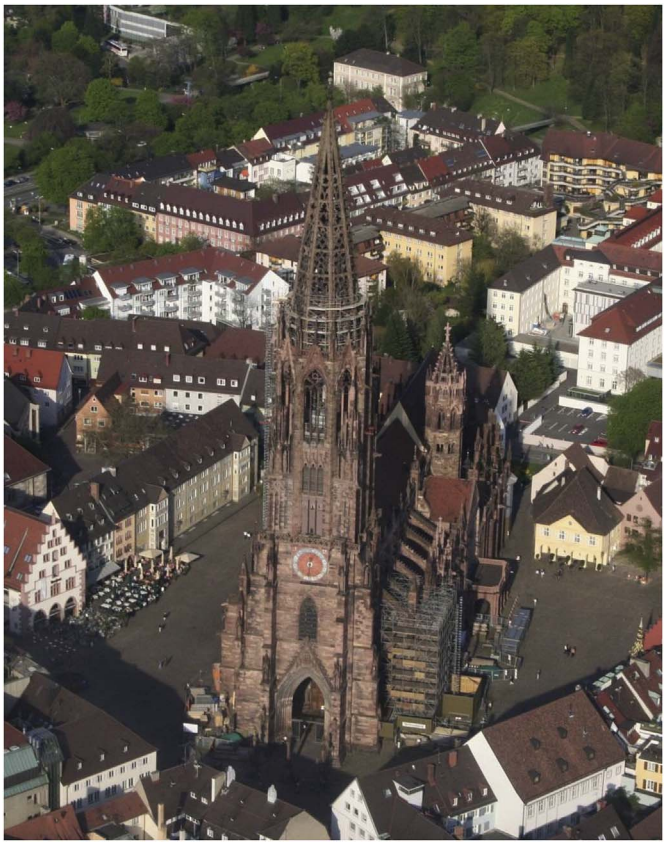

Fig. 1. The Freiburger Münster (Freiburg Minster), Freiburg, Germany. The minster, which was built from around 1200 to 1513, is a well-known cathedral belonging to the Freiburg archdiocese. (Image credit: Von Oberth, CC BY-SA 3.0, https://commons.wikimedia.org/w/index.php?curid=1158443).

This study aims to investigate the chemical composition of these coatings, which belong into the category Type IV of rock varnish (Macholdt et al., 2017), their distribution on the cathedral surfaces, their formation mechanisms, and the source of the Mn at the example of the Freiburger Münster. The minster, which was built from around 1200 until 1513, is a well-known cathedral belonging to the Freiburg archdiocese. Black crusts at the minster were investigated and mapped up to a height of about 30 m together with their chemical composition obtained using a portable XRF, a non-destructive technique that is very suitable for historic buildings and artefacts. In addition, we investigated two samples by optical microscopy, 200-nm fs LA-ICP-MS, Raman spectroscopy, and STXM-NEXAFS, to obtain major and trace element compositions, reveal structures, determine the presence of organisms, and investigate organic functional groups and carbon abundances within the crusts.

2. Material and methods

The Freiburger Münster was investigated at different sites and heights (Fig. 2). Measurements were taken at the Joch 12 S at the Chor (0.5 m height), at the Sterngalerie-Nische south-side (1.5 m height), below the Renaissance-Vorhalle (no silicone resin paint, about 1.5 m height), and at the Schöpfungsportal north-side (2 m height), at the south/east Facade of the “Sterngalerie am Hauptturm” (1.5 m height), at the pillar located at 2/3 on the north-side Sockelbereich (1.5 m height), at the Strebepfeiler 13/14 S (7 m height), at the Renaissance-Vorhalle (south-side) on the gallery (about 7.7 m height), at the

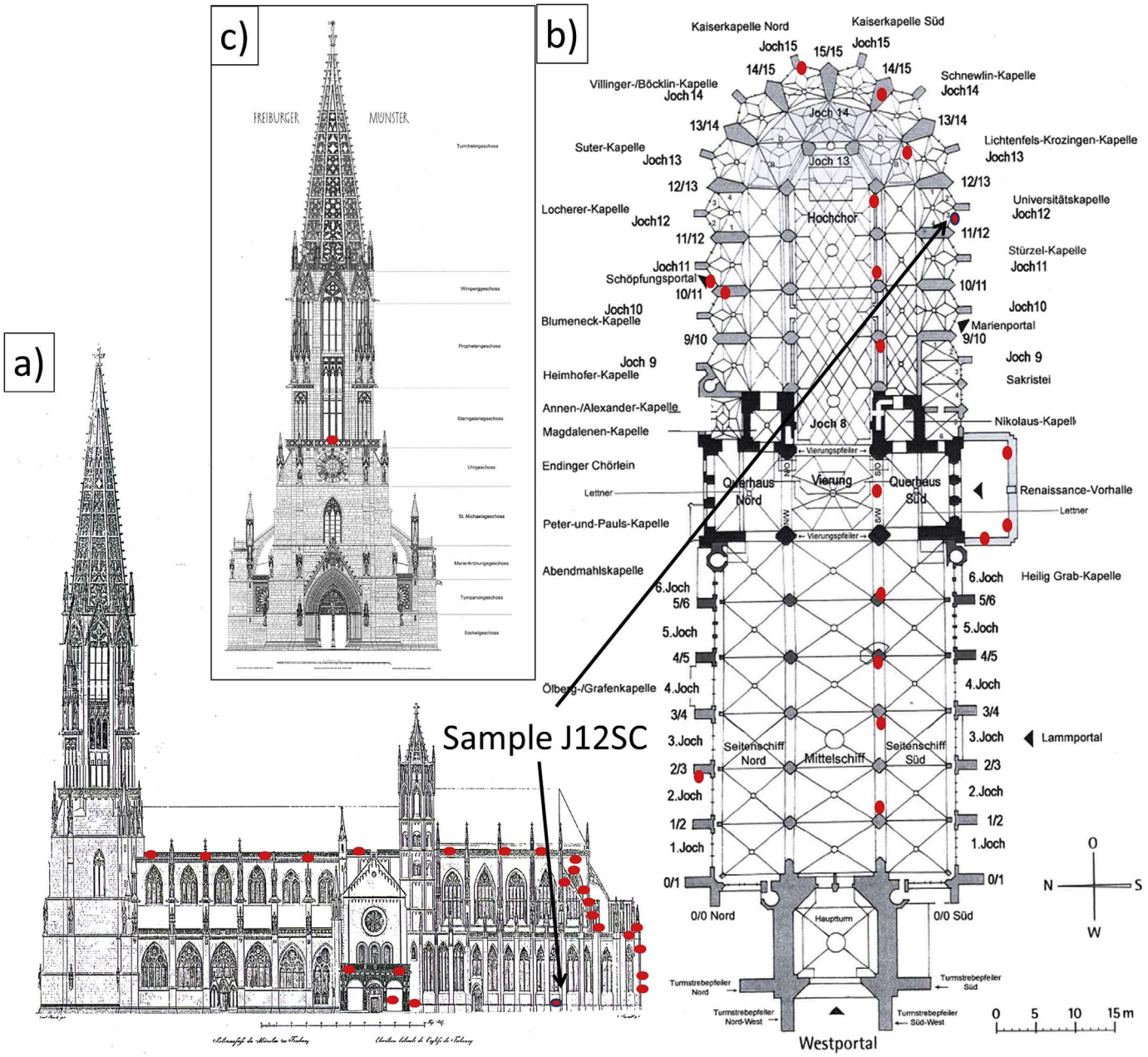

Fig. 2. The South Facade of the Freiburger Münster (a), a cross section (b), and the Hauptturm (c). Marked in red are the main locations where measurements were conducted. (Image credits: Freiburger Münsterbauverein). (For interpretation of the references to colour in this figure legend, the reader is referred to the web version of this article.)

Strebepfeiler 14/15 S (5 m, 7 m, 11 m, 15 m, 17 m, 19 m, and 21 m height), at the Joch 15 N on the Kapellenpfeiler (13 m height), at the Hochchorpfeiler 11/12 N (13 m height), at the Strebepfeiler 10/11 N (13 m height), at the Hochchorwand Joch 13 (13 m and 25 m height), at the southern Hahnenturm (28 m height), at the Sterngalerie east-side (28 m height), and at the Hauptturm (30 m height).

Additionally, the cathedral's building materials were investigated using samples of clean, unexposed rocks to obtain their Mn content (Table 1). The materials from different quarries used as building block resources were Lorettoberger, Heimbacher/Tannenbacher, Schweinstätter, Pfinztäler, Pfaffenweiler, Neckartäler, Fischbacher, and Almendsberger sandstone (Fig. 3, Table 1). The sources of some sandstones are not known, one of them a reference sample called AA1, as well as the sandstone used to build “Chor Nord” and “Turm S-W” (Table 1).

A portable XRF (Thermo Fisher Scientific Niton XL3) was used to investigate the black patches on the Freiburger Münster, especially for the MnO content and the patch distribution. Similar instruments have been used previously for this type of measurements because of their portability and non-destructive operation (Livingston et al., 2016; Uchida et al., 2016; Vicenzi et al., 2016). Measurements were conducted in the “mining” mode, and measurements with each filter were integrated for 20 s. The instrument is equipped with an X-ray source with an energy of 50 keV, a silver anode, and has a spot size of 8 mm. For quality control, the reference material TILL-4 (GeoReM database http://georem.mpch-mainz.gwdg.de) was measured before and after each XRF measurement sequence, as well as between each sample for the calibration curve measurements. A total of one hundred measurements were made on various parts of the Freiburger Münster. The results directly derived from the measurements on the uncoated sandstones are valid as a measure of the Mn concentration in the rock, since sandstones are relatively homogeneous. However, the measurements on

Table 1
Portable XRF measurements of the building blocks from several different quarries and their MnO % content. The numbers in the first column correspond to the numbers in Fig. 2.

# on image	Quarries and descriptions	MnO [%]
1	AA1	< 0.015
2	Above Schöpfungsportal 0–4.1	0.088
3 (a)	Lorettoberger 0–1.3 light colored side	0.042
3 (b)	Lorettoberger 0–1.3 dark red side	< 0.015
3 (c)	Lorettoberger 0–1.3 brown vein	0.041
4	Lorettoberger 0–1.5	< 0.015
5	Lorettoberger 0–1.9	< 0.015
6	Heimbacher/Tannenbacher 0–3.2	< 0.015
7	Heimbacher/Tannenbacher 0–3.1	< 0.015
8	Heimbacher/Tannenbacher 0–2.2	< 0.015
9	Heimbacher/Tannenbacher 0–2.1	< 0.015
10	Schweinstätter	0.074
11	Pfinztäler S 1.1	< 0.015
12	Pfaffenweiler 0–5.1	0.047
13 (a)	Neckartäler A 12.2	< 0.015
13 (b)	Neckartäler A 12.1 on clay filled puddle	0.134
14	Fischbacher 0–7.1	0.035
15	Almensberger A 2.3	< 0.015
16	Chor Nord	< 0.015
17	Turm S-W	< 0.015
18	Yellow Tennenbacher, medieval	0.032

Fig. 3. Sandstone samples from the different quarries that have been used as sources for the building materials for the Freiburger Münster during its construction and restoration. The numbers correspond to the measurement results in Table 1.

the black crusts had to be calibrated differently, since X-rays are produced and scattered back from different depths. Many authors provide the measurement results of thin layers as they were read directly from their portable XRF instrument (Livingston et al., 2016; Uchida et al., 2016). Nevertheless, these authors also state that their numbers are not actual concentrations, but provide relative estimates suitable for comparison only (Uchida et al., 2016; Vicenzi et al., 2016). The depth from which information can be retrieved depends on the atomic number of the element of interest, as well as on the composition of the matrix material, which is in this case the crust and a certain depth of the rock behind it.

To obtain a calibration curve appropriate for the Mn coatings, we used four Mn-covered rock samples (rock varnishes from California). Squares cut from these rocks were used to obtain crust-covered surfaces between 4.38 and 6.25 cm^2. The exact surface areas were determined utilizing the software ImageJ. The Mn-rich crusts were measured by portable XRF on 21 different spots on each rock used for calibration, since the thickness of the crust varies across the rock surface. An average value was taken for the calibration. Additionally, the underlying rocks on the backside of the squares were measured to obtain the MnO contents of the host rocks.

The crusts were dissolved off the rock surface by treatment with 0.02 M hydroxylamine hydrochloride at a pH of 2.5 and a temperature of 70 °C. The solution was evaporated and the procedure repeated several times until XRF measurements on the formerly MnO-covered surface gave values similar to those of the host rock. The solution was heated until the dissolved crust material precipitated, the precipitate was weighed and dissolved in 2% HNO_3. This solution was measured by ICP-MS (Agilent 7900 ICP-MS) for its Mn content, with Rh as the internal standard element. The reference materials BHVO-2 and BCR-2 (Jochum et al., 2016) were additionally measured for quality control. The Mn surface density (i.e., the amount of Mn per surface area) was calculated using the sample surface area and mass of Mn in the sample obtained from the dilution factor and the Mn mass fractions measured by ICP-MS. In addition to the calibration values derived by this method, we also used a standard foil from Micromatter™ with a Mn loading of 104.7 µg cm^{-2}. The Mn K-α count rate (peak height) obtained by the XRF from this standard foil, showed significant differences depending on whether it was measured in air or with a rock slice (basalt or quartzite) behind it (Fig. 4). We consider the values obtained with the rock backings as the most appropriate for our measurements on Mn crusts. Plotting the Mn surface density against the Mn K-α count rate of the four rock varnish samples and the standard foil with the rock backings, we obtained a calibration curve (Fig. 4). In principle, a non-linear function should be chosen since the detection is a non-linear process with high count rates for surface detections and no influence of the element contribution below the information depth. The calculation of the calibration curve can thus be based on an adaption of the theoretical equation by Barrea et al. (1998), resulting in a logarithmic fit. From our two measurement points with very high Mn values, which we derived from the Renaissance Portico, we were able to calculate the extreme of the logarithmic function and use it to fit the data (Fig. A of the appendix). However, since we do not have more measurement points of high values, such an extrapolation is problematic. Therefore,

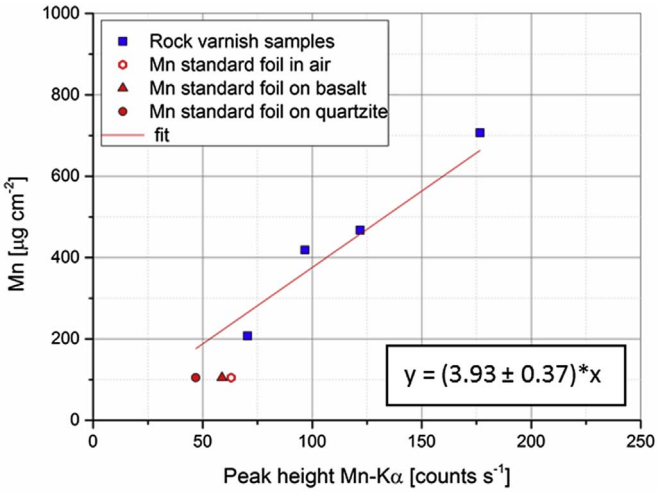

Fig. 4. Calibration curve produced by linear fit to obtain Mn surface densities (masses per area) from measurements by portable XRF. The four blue squares are measurements from leaching experiments using rock varnish crusts. The red symbols represent the measurements obtained from a Mn standard foil produced by Micromatter™ in air (open circle), with a quartzitic background material (filled circle), and with a basaltic background material (triangle). The measurement of the foil in air was excluded from the fit since it does not represent the conditions of a Mn-crust on a host rock. (For interpretation of the references to colour in this figure legend, the reader is referred to the web version of this article.)

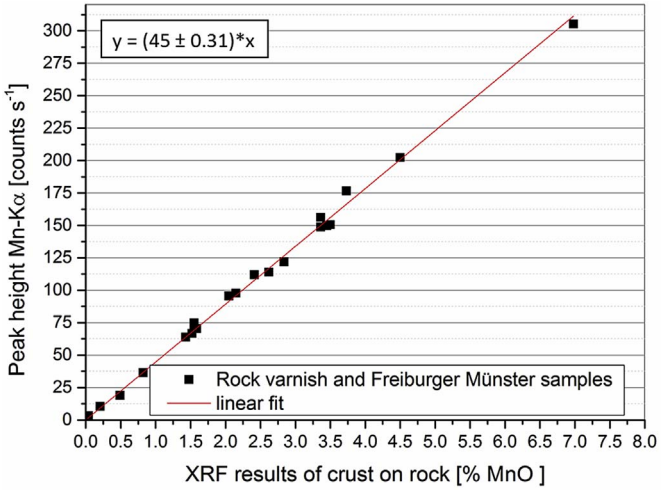

Fig. 5. Plot of the peak height of Mn K-α versus the apparent Mn concentration reported by the portable XRF.

and because the logarithmic fit does agree very well with a linear fit in the range where most of the measured points are located (Fig. A of the appendix), we chose to use the linear function to calculate our data. Our results are in accordance with previously published numbers of 150–300 μg cm^{-2} Mn on varnish crusts measured by Reneau (1993).

Since the portable XRF reports its results in the form of an apparent concentration rather than as count rates, we evaluated the relationship between count rate and reported concentration (Fig. 5). We found that as long as the host rock matrix is more or less the same (sandstone in our case), the correlation is excellent, and the apparent concentrations can be used for convenience to convert the XRF measurements into surface densities. On the other hand, our measurements with the standard foil indicated a significant influence of the host rock matrix. Therefore, calibrations using host rocks similar to the samples or the use of the count rates obtained from the spectra are a prerequisite for accurate results.

In one sample, J12SC, taken from Joch 12S at the Chor at 0.5 m height, 39 elements were measured by a 200-nm fs LA-ICP-MS (a ThermoFisher Element 2 single-collector sector-field ICP-mass spectrometer combined with an ESI 200-nm fs-laser ablation system NWRFemto) to obtain accurate mass fractions of major and trace elements with low detection limits. As reference materials, GSE-1G and NIST 610 (GeoReM database http://georem.mpch-mainz.gwdg.de) were chosen. Laser ablation was conducted in a New Wave Large Format Cell in a He atmosphere. All measurements were conducted using the medium mass resolution mode (2000) with flat-top peaks. The sample was introduced as a thick-section (70 μm) of the cross section of the crust. After pre-ablation the sample was scanned via line scans along a profile from the underlying rock through the varnish into the embedding resin. To normalize the data, the oxides of the major elements (Na_2O, MgO, Al_2O_3, SiO_2, P_2O_5, K_2O, CaO, TiO_2, MnO_2, and Fe_2O_3) were assumed to add up to 98%. By this method, the procedure is reproducible and easily recalculated if future measurements are able to provide the exact amount of water and organics within the crusts.

Furthermore, sample J12SC and reference compounds were investigated by STXM-NEXAFS with the X-ray microscope at beamline 5.3.2.2 at the Advanced Light Source (ALS), Berkeley, CA, USA, and with the MAXYMUS microscope at BESSY II, Helmholtz-Zentrum Berlin, Germany, to obtain element distribution maps and to study the functional groups of the organic matter distributed within the sample. A description of the STXM-NEXAFS technique can be found in Moffet (2011). Since STXM-NEXAFS is a transmission light method and requires samples of a thickness of about 100 nm, focused ion beam (FIB) sputtering (milling) was performed at the Max Planck Institute for Polymer Research (Mainz, Germany) using a Nova600Nanolab FIB dual-beam instrument of FEI to prepare an ultra-thin section of the sample (50 μm × 30 μm x 150 nm). Details on the X-ray microscopes can be found in Kilcoyne et al. (2003) as well as Weigand (2014) and Follath et al. (2010). The STXM measurement and sample handling techniques are described in Pöhlker et al. (2012).

The same sample was used to conduct micro-Raman spectroscopy. Raman spectra were obtained using a Bruker Senterra Instrument at the Max Planck Institute for Polymer Research (Mainz, Germany). The measurements were made with a 785 nm laser and an objective of 50× magnification. The spot size was about 2 μm, 2 acquisitions were chosen, and an aperture of 5 × 1000 μm. The spectral range from 0 to 3500 cm^{-1} was measured with a resolution of 3–5 cm^{-1}. The power was increased from 1 mW, over 10 mW, up to 25 mW, and exposure times between 90 and 180 s were chosen, using the settings published by Sadezky et al. (2005) for orientation. Since the sample was very thin (100–200 nm), the high power settings eventually destroyed the sample. To validate the data, additional measurements were conducted on an unprocessed piece of sample J12SC, with 10 mW, an objective of 20× magnification, and a spot size of about 4 μm. The same bands were detected at the same wavenumbers, indicating that the bands were not produced by degradation of the sample material by the laser. Baseline correction was performed with the software OPUS 7.5 Senterra E. A concave rubberband correction with 10 iterations for 64 baseline points was conducted. Uncorrected raw spectra are provided in Fig. B of the appendix.

3. Results and discussion

3.1. Sandstones as possible source of Mn

Measurements were conducted to obtain an overview over the Mn abundances in the materials used for the construction of the minster (sandstones) (Table 1) and the presence of Mn in the crusts on the minster's facade (Table 2). Several bare sandstones were measured at the facade, as well as freshly-cut sandstone surfaces from several quarries that had been used as sources for the sandstone blocks of the minster. The sandstone matrix measurements revealed MnO mass fractions between < 0.015% (below the detection limit) and 0.088%. Small clay lenses (up to 1 cm in diameter) within one sandstone sample had MnO mass fractions up to 0.13% MnO.

Black patches at the minster's facade were measured from 0.5 m to about 30 m in height. Manganese-rich patches (≥150 μg cm^{-2}) were only found up to a height of 7 m. The Mann-Whitney-U test (Mann and Whitney, 1947), conducted using the software SPSS, was used to ascertain that the difference between the Mn-abundances of the patches below and above 7.7 m was indeed significant. This was confirmed by the test ($U = 14$, $p < 0.0005$). The effective size index calculated for the dataset ($r = 0.73$) after Cohen (1992) also corresponds to a strong effect. The exception were especially Mn-rich patches at the Renaissance-Vorhalle (Renaissance Portico) at a height of about 7.7 m, a supplement to the minster, which had been treated during restoration work (2003) with a silicon resin. Visually similar black patches were found at greater heights, but they all lacked high Mn mass fractions. They either showed elevated amounts of CaO (~20%) and S (~6%), or biological encrustations. While high Ca and S mass fractions of black patches indicate a gypsum crust ($CaSO_4*2H_2O$) which captured soot particles, the organisms found were identified as black fungi and cyanobacteria (Fig. 6C–D). Black fungi (De Oliveira et al., 2011; Gorbushina et al., 1993; Saiz-Jimenez et al., 2012; Viles and Gorbushina, 2003), cyanobacteria (Bonazza et al., 2007b; Uchida et al., 2016), and black gypsum crusts (Bonazza et al., 2005; Brimblecombe and Grossi, 2009; Grossi and Brimblecombe, 2002; Ruffolo et al., 2015) have been previously observed forming black crusts on rock surfaces. However, it cannot be distinguished by macroscopic features alone, if the black patches are soot, fungi, or Mn-rich crust, while they do clearly

Table 2
Portable XRF measurements of the Freiburger Münster facade. Several measurements were taken at each location, only the highest values are given.

Location	maximal XRF percentages received (% MnO)	peak height Mn-Kα	Mn per area [μg cm^{-2}]	height above ground [m]
J12SC, Joch 12 S-Chor	3.36	149	580	0.5
S-E Facade Sterngalerie am Hauptturm	< 0.015	n.d.	n.a.	1.5
Pillar 2/3 north-side Sockelbereich	3.36	156	610	1.5
Sterngalerie niche, south-side	0.027	2.88	11	1.5
Below the Renaissance Vorhalle	3.45	150	590	1.5
Schöpfungsportal north-side	2.62	114	450	2
Strebepfeiler 14/15 S	1.43	63.7	250	5
Strebepfeiler 14/15 S	1.52	66.8	260	7
Strebpfeiler 13/14 S	1.55	74.8	290	7
Rennaissance-Vorhalle	6.98	305	1200	7.7
Strebepfeiler 14/15 S	< 0.015	n.d.	n.a.	11
Joch 15 N, Kapellpfeiler	< 0.015	n.d.	n.a.	13
Hochchorpfeiler 11/12 N	< 0.015	n.d.	n.a.	13
Strebepfeiler 10/11 N	< 0.015	n.d.	n.a.	13
Strebepfeiler 14/15 S	< 0.015	n.d.	n.a.	15
Strebepfeiler 14/15 S, west-side of column	< 0.015	n.d.	n.a.	15
Strebepfeiler 14/15 S, east-side of column	< 0.015	n.d.	n.a.	17
Top of the Strebepfeiler 14/15 S	< 0.015	n.d.	n.a.	19
Strebepfeiler 14/15 S towards Hochchor	< 0.015	n.d.	n.a.	21
Hochchorwand, Joch 13	0.821	36.5	140	23
Hochchorwand, Joch 13	0.206	10.5	41	25
Along the facade of the Münster	< 0.015	n.d.	n.a.	28
Southern Hahnenturm inner side	0.028	3.5	14	28
Southern Hahnenturm outer side	< 0.015	n.d.	n.a.	28
Sterngalerie east-side	0.038	3.4	13	28
Hauptturm	< 0.015	n.d.	n.a.	30

show different chemical compositions (Fig. 7).

Previous authors had discussed whether the Mn-rich crusts on facades might obtain their elements by leaching of the underlying sandstone, transport through the sandstones pore systems, and deposition at the surface (Grüner et al., 2011). Most sandstones used to build the minster have MnO concentrations below the detection limit of the portable XRF used (0.015% MnO). Thus, to obtain enough Mn to form a crust of 3.4% MnO (J12SC) from a sandstone with < 0.015% MnO, transport of all available Mn present in the sandstone from a depth of at least 5 cm to the surface would be necessary. This depth is indeed in the range where capillary rise can occur in porous sandstones (Tsunazawa et al., 2016). However, no Mn-lined fissures are observable in cross sections and the crusts seem to be continuous layers and not predominantly abundant close to pore systems or intruding the rock surface similar to weathering crusts (Fig. 8g, h). The patch distribution could be explained by proximity to areas with higher porosity, however, the height limitation of Mn-rich patches to below 7 m, the leaching process within the sandstones, and the preferred accumulation of Mn^{4+} over Fe^{3+} could not be explained. It is not clear how Mn could be mobilized within the sandstones, which would require low pH or reducing conditions, and which processes would allow the precipitation and oxidation of Mn^{2+} to immobile Mn^{4+} at the rock surface. Another good indicator that such a leaching process is probably not the main driving force behind the development of the crusts is the fast and preferential growth on top of sealing paints that had been applied on particular sandstone surfaces after restoration.

Table 3
Results from 200-nm fs LA-ICP-MS measurements of sample J12SC (taken from Joch 12 S at the Chor at 0.5 m height; Fig. 2a, Table 2).

Element	Isotope used	Sample J12SC		Element	Isotope used	Sample J12SC	
		[μg g^{-1}]	RSD [%]			[μg g^{-1}]	RSD [%]
Na	Na^{23}	1840	42	Cs	Cs^{133}	11	23
Mg	Mg^{25}	3520	34	Ba	Ba^{138}	1750	27
Al	Al^{27}	43600	26	La	La^{139}	20	51
Si	Si^{29}	253000	18	Ce	Ce^{140}	42	33
P	P^{31}	25900	50	Pr	Pr^{141}	5.3	48
K	K^{39}	20400	26	Nd	Nd^{143}	20	41
Ca	Ca^{43}	20100	28	Sm	Sm^{147}	4.6	36
Ti	Ti^{47}	1550	23	Eu	Eu^{151}	1.1	28
V	V^{51}	83	37	Gd	Gd^{157}	4.9	23
Cr	Cr^{53}	64	22	Tb	Tb^{159}	0.73	37
Mn	Mn^{55}	77100	39	Dy	Dy^{161}	4.4	37
Fe	Fe^{57}	29100	30	Ho	Ho^{165}	0.81	31
Co	Co^{59}	525	71	Er	Er^{167}	2.4	30
Ni	Ni^{60}	286	39	Tm	Tm^{169}	0.31	29
Cu	Cu^{63}	328	28	Yb	Yb^{173}	2.2	39
Zn	Zn^{67}	5000	36	Lu	Lu^{175}	0.28	39
Rb	Rb^{85}	83	31	Pb	Pb^{208}	8300	30
Sr	Sr^{88}	510	28	Th	Th^{232}	7	34
Y	Y^{89}	17	28	U	U^{238}	3.3	23
Zr	Zr^{90}	35	38				

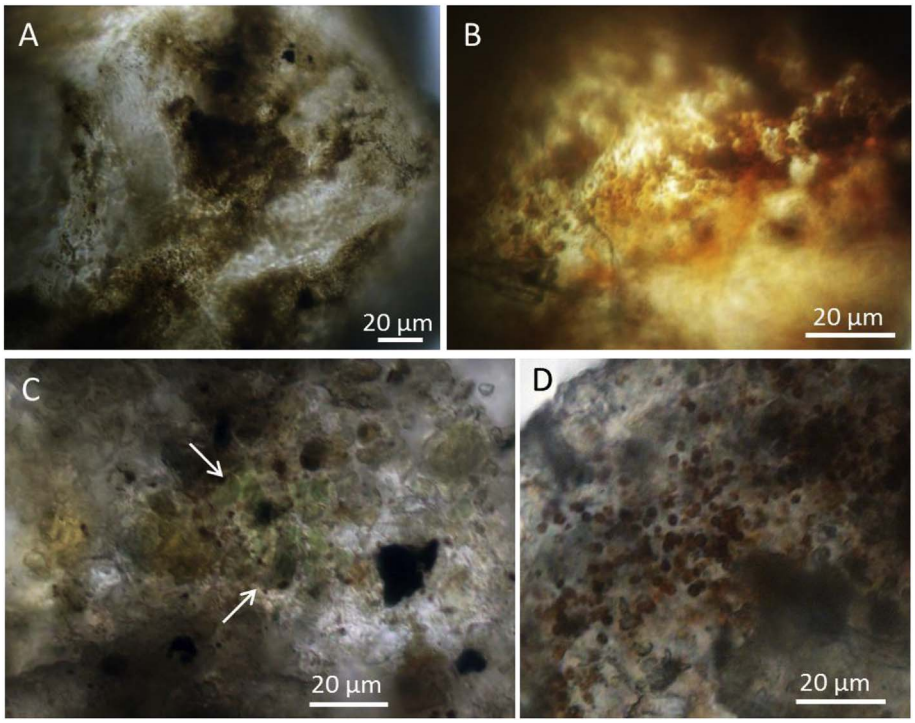

Fig. 6. Light microscopy of material from the Freiburger Münster. A) dark brown to black stains on rocks originating from soot, Mn-, and Fe accumulation (630 µg cm^{-2} Mn); no fungal hyphae or cellular pigments are visible. B) orange, carotenoid-like and brown pigments within cell-like structures on the same sample. Images A and B were taken from a sample from Joch 12 S am Chor (J12SC), at 0.5 m height (Fig. 7d, Table 3). C) cyanobacteria (arrow) on rocks originating from the "Sterngalerie" (Mn mass fraction below the detection limit). D) brown fungal cells and hyphae originating from the "Sterngalerie". (For interpretation of the references to colour in this figure legend, the reader is referred to the web version of this article.)

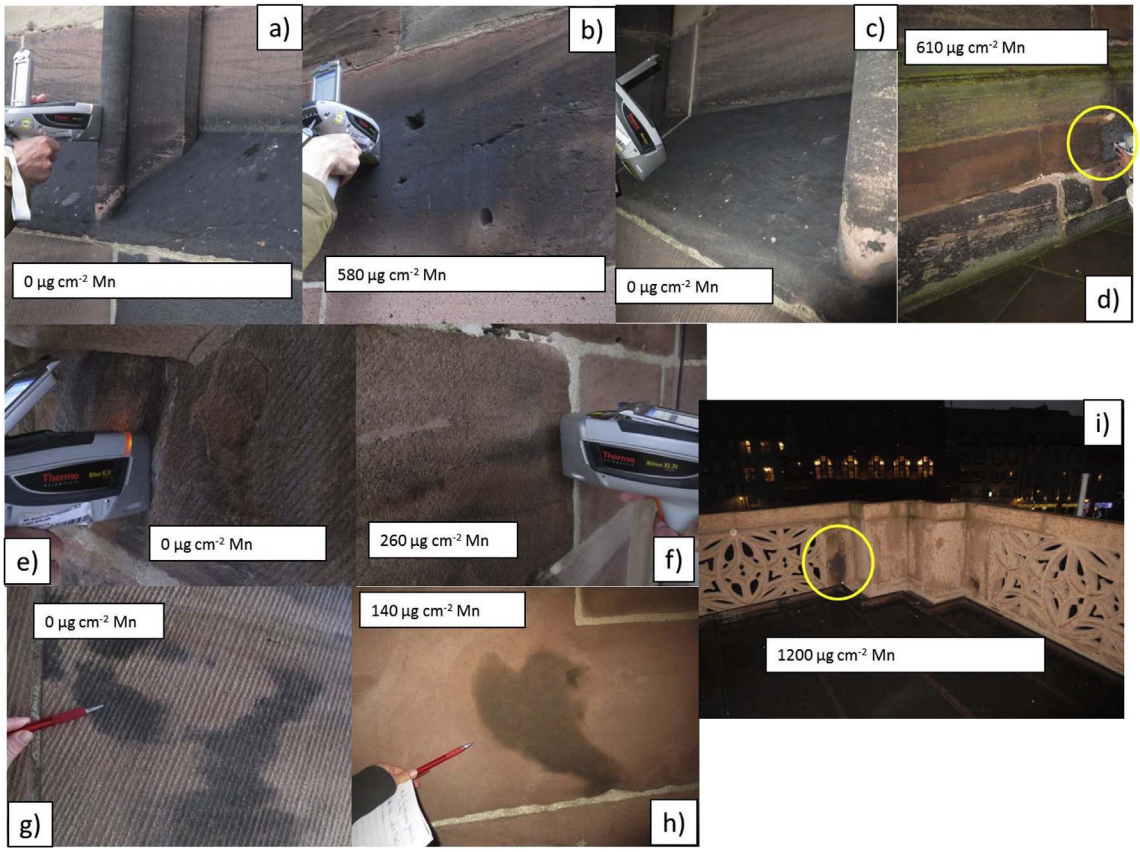

Fig. 7. Measurement spots and measured Mn surface densities. One cannot distinguish visually if the black patches are soot, fungi, or Mn-rich crusts. Sample J12SC was taken from the area shown in d).

3.2. Vehicle emissions as potential sources of Mn

Another possible source of Mn is pollution by traffic or similar sources, which could explain the acceleration of crust growth in recent times. Motor vehicles are known to be a major source of particulate matter and contribute strongly to the distribution of metal-containing particles in urban air (Schauer et al., 2006). The abundance of Mn in air masses in larger German cities is about 20 ng m^{-3}, based on Vallero

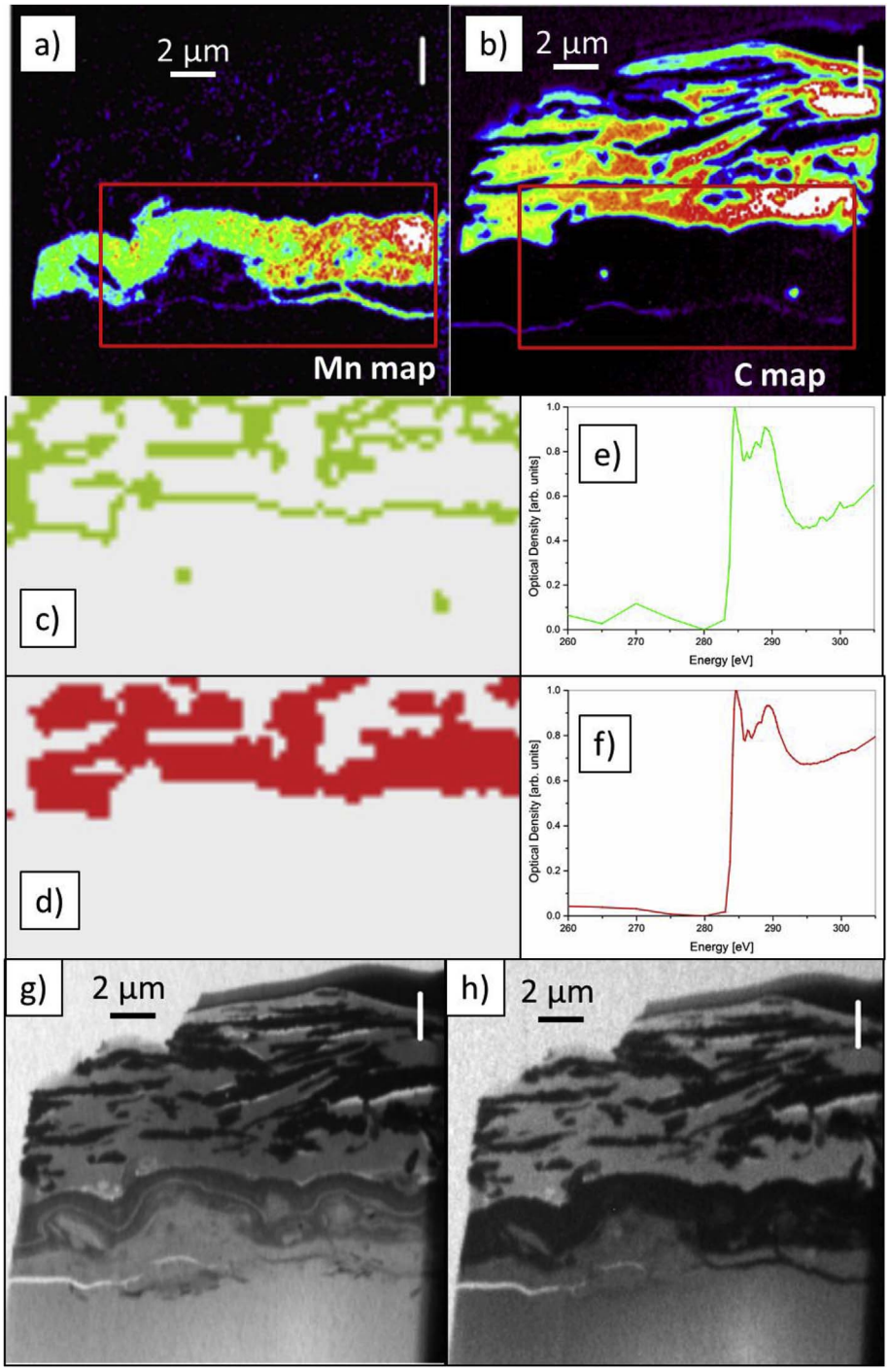

Fig. 8. Element maps of Mn (a) and C (b) obtained by STXM—NEXAFS measurements. Cluster analyses of the range of energy in which carbon absorbs (260–305 eV) show two C-rich clusters (c, d), with strong absorption bands (e, f) indicating the presence of soot. These two clusters show that the carbon from underneath the Mn-rich crust shows the same functional groups as the carbon deposited on top of the crust and might therefore only be introduced below the Mn-layer through cavities. The carbon clustering was conducted for the area marked by a red box in (a, b). Fig. 7(g) is a structure overview image at the Mn pre-edge (530.5 eV) and (h) an overview at the absorption energy of Mn (641 eV). (For interpretation of the references to colour in this figure legend, the reader is referred to the web version of this article.)

(2014) and M. Shafer (personal communications, 2016). Since the addition of Mn to gasoline was restricted in Germany to 6 mg l^{-1} by January 2011, and to 2 mg l^{-1} by January 2014, according to § 3 (5) of the Kraftstoffverordnung 2012, Mn gasoline additives are not a significant source of Mn to air in Germany. However, other traffic related sources are relevant. An average car produces 10–200 µg km^{-1} Mn per km driven (particles < 10 µm), most of which is released by wearing down and evaporation of brake material (0.1–0.17% of the dust produced by brake material < 10 µm is Mn), to a lesser extent from resuspended road dust (up to 700 µg g^{-1} of the resuspended road dust is Mn), and only marginally from tailpipe emissions (22–74 µg g^{-1} of the tailpipe emission is Mn) (Schauer et al., 2006). Regarding the particle size distribution, information diverges. While Schauer et al. (2006) state that Mn-rich particles are most abundant in the size range between 1 and 10 µm, with the highest mass abundance between 1 and 1.8 µm, Birmili et al. (2006) found during their studies that particles < 0.5 µm and > 1.5 µm are the main Mn contributors in the fine and coarse particulate matter (PM) size ranges. They interpret the observed spread across all size ranges as an indicator for the existence of several different source mechanisms.

Since mechanically generated particles are relatively coarse in size, normal grinding of brake material cannot be the sole mechanism of brake wear emission (Schauer et al., 2006). Since brake pads contain organometallic material (Rogge et al., 1993), friction-heated surfaces of brake pads and rotors are most likely to also contribute to the PM production by volatilization and condensation of this material (Garg

et al., 2000; Sanders et al., 2002). Tire material does not contribute to Mn emissions, but it releases Zn in relatively large amounts (Schauer et al., 2006). The high Zn mass fractions (5000 μg g^{-1}) in the crusts measured on the Freiburger Münster are thus an additional indicator for vehicles as PM sources (Table 3). Other traffic-related elements of high abundance in the crusts on the Freiburger Münster are Pb (8300 μg g^{-1}) and Ba (1750 μg g^{-1}) (Table 3).

Brake pad wear is also the dominant contributor to Ba in urban air, since barium sulfate is a major component of them. Barium sulfate is used as a stable filler that accounts for up to 40% of the brake pad weight (Blau, 2001). Unlike U.S. American and Japanese vehicles, European vehicles' brake linings are usually comprised of low-steel or NAO materials due to higher performance requirements (Birmili et al., 2006). They consist of steel (0–20%), Cu (16%–22%), Al_2O_3 (0–2.5%), Fe_2O_3 (0–10%), ZnS (5–6%), $BaSO_4$ (10%–16%), and organic binding materials, according to the "Bremsenhandbuch" (brake handbook) (Breuer and Bill, 2006). The largest Ba mass fractions can be found in PM > 10 μm, since they form by mechanical abrasion (Schauer et al., 2006). Barium was found to have an abundance of about 3.5–17.1 ng m^{-3} in urban air (Schauer et al., 2006).

Lead can be emitted from several sources, including fuel and motor oil combustion, brake wear, and re-suspension of enriched road dust (Cadle et al., 1997; Garg et al., 2000; Young et al., 2002), among which resuspended road dust predominates (Schauer et al., 2006). A major fraction of the Pb in road dust still has its source in industrial and tailpipe emissions from the time before the phase-out of leaded gasoline, but also from Pb wheel alignment weights that are lost from vehicle wheels and subsequently pulverized by traffic (Root, 2000). Since tetraethyl lead, the former organometallic additive to gasoline, tended to oxidize and damage valves, spark plugs, and combustion chambers, brominated and chlorinated organics were added as scavengers (Robert, 1984). These compounds convert Pb oxides to volatile halide salts which exit through the tailpipe (Nriagu, 1990). Because these compounds are resistant to removal, they are still common in the environment despite the lead phase-out policy (Oudijk, 2010). Currently, Pb concentrations of 1–9 ng m^{-3} were measured in urban air in Milwaukee and Waukesha, WI, USA and Denver, CO, USA (Schauer et al., 2006). The agreement of the main inorganic particulate matter released by vehicles and the main enrichments of elements within the crusts suggests that vehicle emissions are indeed good candidates for the sources of the Mn, Ba, Pb, and Zn observed on the Freiburger Münster. Antimony would be another element providing information about the source of the elements (Iijima et al., 2008; Okkenhaug et al., 2015), and should be measured additionally in future studies.

3.3. Manganese leaching and distribution

Manganese produced and released through the processes described above has an average leachable fraction of 90% (at 37 °C, pH ~7.4, and leaching for 8 h) (Schauer et al., 2006). For comparison, Fe has only a leachable fraction of 10–25%, which is in agreement with the enrichment of Mn over Fe in the minster's crusts, even though the elements generally have similar chemical behavior. Barium and Pb have a leachable fraction of about 25%, and Cu, Zn, and Sb 50–60% (Schauer et al., 2006). While Janssen et al. (1997) also found a solubility of 91% for Mn in a weak acidic solution, Espinosa et al. (2002) and Birmili et al. (2006) determined a solubility of 10–40% in a pH-neutral water solution. However, since rain tends to be slightly acidic, it is likely that most of the Mn in aerosols is soluble in urban environments. Leaching and redeposition of aerosol Mn is thus a plausible mechanism for the enrichment of Mn on the facade of the Freiburger Münster. An explanation for the decrease of Mn with height can be the vertical distribution of vehicle emissions. The highest exhaust fume amounts are reported close to the ground, rapidly decreasing at greater heights (DePaul and Sheih, 1985). The exact height up to which vehicle movements influence the flow and turbulence of air masses, and by this the distribution of vehicle emissions, depends on the width and height of the street canyons within a city, as well as on wind speed, tree density, and other factors. Turbulent air masses, responsible for the distribution of the vehicle emissions, are reported to reach up to 7–12 m (DePaul and Sheih, 1985; Qin and Kot, 1993). This relation between the concentration of heavy metals in black crusts and the distribution height of vehicular traffic emissions was observed before by Ruffolo et al. (2015).

The limitation of the Mn-rich patches to sandstone buildings, while not affecting houses that are close by, has puzzled authors before (Vicenzi et al., 2016). One possible explanation is the availability of alkali and alkaline earth metal containing minerals within sandstones, which increase the pH value. The rough surface, which prevents water from draining and has a tendency to remain cold and delay evaporation or even initiate condensation of water, could also contribute. The discolorations on the facade of the Freiburger Münster show a patchy shape, often starting in the middle of the sandstone blocks. This is in agreement with the observation that during warmer days, condensation can occur preferentially in the middle of the sandstone blocks where the material is surrounded by rock in five of six directions. Rock surfaces are known to be favorable sites for condensation from the atmosphere (Duvdevani, 1949, 1953), providing an additional water source that is not available to the rest of the sandstone block. Furthermore, clay layers are abundant within sandstones, containing minerals that store water in their interlayer sites. The water film deposited on the rock surface will initially have slightly to strongly acidic pH values, similar to the pH value of rain or fog in urban areas. Upon deposition, the pH value of the water film increases due to the exposure to alkali and alkaline earth metal containing minerals within the sandstone. Furthermore, protons can be absorbed by clay minerals, releasing cations to the water film, increasing the pH value of the solution.

A Pourbaix diagram (E_h-pH diagram) can be utilized to determine the conditions needed for the oxidation from Mn^{2+} to Mn^{4+} (Fig. C of the appendix). Increasing the pH value from 6 (rain water) to about 8–9 (addition of alkaline paint, alkaline catalysts from paint, alkali and alkaline earth metal oxides, or carbonates) shifts the system from the stability field of mobile dissolved Mn^{2+} into the stability field of immobile solid γ-MnOOH(s) or δ-MnO_2(s) (Brookins, 2012; Takeno, 2005). Thus, a phase boundary is crossed in the Pourbaix diagram and the immobile Mn^{4+} phase is thermodynamically favored (Fig. C of the appendix). However, Mn^{2+} can persist metastably in solution for years in the absence of catalysts or biogenic oxidation. Nevertheless, when water evaporates, the Mn activity increases and the solid Mn stability field, or range of conditions where Mn^{4+} is stable, shifts towards lower pH and E_h conditions (Hem, 1963). Thus, the transformation from Mn^{2+} to Mn^{4+}, even in the absence of a catalyst, becomes more likely (Martin, 2005). Manganese^{4+} can then precipitate and form stable, immobile Mn oxyhydroxide phases. Since each sandstone block at the minster is different in its mineral distribution and content, this could result in the observed, seemingly randomly distributed, crust-free and crust-covered rock surfaces. To confirm this assumption, chemical and mineralogical analyses of the sandstones themselves would be necessary.

The oxidation might not only take place as homogeneous oxidation, as described above, but also as heterogeneous oxidation, e.g., when it is catalyzed by a metal oxide surface. These surfaces can either be those of foreign minerals, but in the case of manganese, autocatalysis can also contribute significantly, e.g., Mn^{2+} can be oxidized to additional MnOOH on an MnOOH surface (Martin, 2005). That is, the system catalyzes itself, increasing the reaction rate as the reaction proceeds, leading to the occurrence of Mn as patches, which can become explainable by this process. Manganese oxidation can also be catalyzed by bacteria, fungi, and other organisms; however, microorganisms (fungi and cyanobacteria) were only found in Mn-poor regions at the Freiburger Münster (Fig. 6C–D). No microorganisms could be verified on the Mn-rich patches (Fig. 6A–B). Most Mn-rich crusts developed in

areas that have a high water throughput. This indicates that water, or rather particles dissolved or leached in water, are a probable source for the Mn mass fractions, a theory also proposed by Livingston et al. (2016) for urban Mn crusts. However, the patches observed below the Renaissance-Vorhalle can only result from splash water or condensed water as sources, since they are not directly exposed to rain, indicating the importance of splash and condensation water deposition.

3.4. Wet vs. dry deposition mechanisms

Air pollutants are deposited or transferred to materials surfaces through two mechanisms referred to as "wet" and "dry" deposition (Everett et al., 1988). Wet deposition occurs when pollutants are brought down dissolved in rainwater, whereas dry deposition refers to processes through which a pollutant is deposited directly on surfaces (Grossi and Brimblecombe, 2002). Dry deposition happens all the time, while wet deposition is due to precipitation and consequently is an intermittent event with both spatial and temporal variations (Grossi and Brimblecombe, 2002). To calculate the dry deposition rate of Mn at the Freiburger Münster, the absolute abundance of Mn in air masses around Freiburg is of importance. This Mn abundance was reported to be about 20 ng m^{-3} in larger German cities, based on Vallero (2014) and M. Shafer (personal communications, 2016). The dry deposition rate also depends on the dry deposition velocity, which depends on the particle size, shape, aggregation, density, the Reynolds number of the flow, and the surface roughness of the deposition material (Pesava et al., 1999; Sehmel, 1980). Since the minster's walls are highly structured by blocks of stone, ornaments, and sculptures, the flow over these surfaces does not form a simple turbulent boundary layer (Pesava et al., 1999). To understand dry deposition velocities on sandstone facades, one has to consider the rough surface with complex geometry creating a separated boundary layer (Pesava et al., 1999). The dry deposition is higher for rough sandstone surfaces than for smooth surfaces (Pesava et al., 1999; Sehmel, 1980), and the deposition velocity depends on the orientation, structure, and location of the surface. Edges and corners have higher deposition rates than surfaces in the middle of the building. On average, the deposition rate of particles with about 0.6–0.8 μm mean diameters on cubic sandstone features with 0.2 mm roughness height are in the range of 0.03–0.14 cm s^{-1} with an average of about 0.05 cm s^{-1} (Pesava et al., 1999). Flat surfaces produce significantly lower deposition velocities (about 0.005 cm s^{-1}) and the deposition speed increases rapidly for a surface roughness of > 0.15 mm (Pesava et al., 1999). Using these values and an average Mn concentration of 20 ng m^{-3}, the dry deposition rate for Mn at the Freiburger Münster can be calculated to be in the range of 20–90 ng cm^{-2} a^{-1}, depending on the exact position of the sandstone square. However, these values were calculated for particle sizes in the range between 0.1 and 1 μm, where the deposition velocity is lowest and only a weak function of the particle size (Guha, 1997). Since Mn-rich particles released by vehicular traffic are up to 1.8 μm in size, these numbers are probably underestimations of the actual deposition velocity. As an example, by using the values above, it would take about 1360–6300 years to grow a crust of 120 μg cm^{-2} solely by dry deposition, indicating that wet deposition must play an important role.

To obtain the wet deposition rate, we use the wet scavenging ratio of about 10^6 for Ca (concentration in rain divided by the concentration in air) (Hicks (2005) and the average annual precipitation in Germany (about 1000 mm). This provides Mn wet deposition rates of about 2 μg cm^{-2} a^{-1}, and the crust's accumulation would thus take about 60 years. This calculated value is significantly higher than the Mn wet deposition value calculated by Conko et al. (2004) for Reston, Virginia, USA. They found Mn wet deposition rates of 0.2 μg cm^{-2} a^{-1}. However, these values were calculated based on measurements in Reston in 1998, a suburb of Washington D.C. The reported Mn abundance at the Washington monument (city center of Washington D.C.) was only about 2 ng m^{-3} in 1992 and 2.5 ng m^{-3} in 1993 (Wallace and Slonecker, 1997), about a ten times lower than the Mn abundance in air reported from large German cities. The calculated wet deposition rate of about 2 μg cm^{-2} a^{-1} in Freiburg can hence be considered as reasonable.

However, even these wet deposition values are almost too low to explain the crust accumulation at the minster, requiring some 60 years for the buildup of a crust with 120 μg cm^{-2} of Mn. Since both wet and dry deposition take place in parallel, the deposition rates can be added up, and additional condensed water on sandstones and clay mineral incorporations in the sandstone can slightly increase the dry deposition rates. Deposition of soluble materials occurs more readily on moist surfaces (Grossi and Brimblecombe, 2002), and clay minerals are able to fix relatively large amounts of Mn, depending on the pH and E_h conditions (Reddy and Perkins, 1974). It seems very likely that manganese oxides are initially present as external coatings onto typical clay minerals such as illite and bentonite (Potter and Rossman, 1977). Therefore, autocatalysis, in combination with wet and dry deposition, the abundance of clay minerals, and regular condensation of water at the stone surfaces, are factors that can contribute to explaining the crust's accumulation.

3.5. Trace elements and organics in the crusts

The fs LA-ICP-MS results revealed that elements easily scavenged by Mn oxyhydroxides are enriched in the black crusts (Table 3). Their composition is similar to that of common rock varnish, but reveals several differences, e.g., lower Ce and Fe mass fractions and significantly higher Mn values. Especially interesting is the lack of the positive Ce anomaly that is usually associated with Mn oxyhydroxides, such as rock varnish. Since Ce is the only rare earth element (REE) that can be oxidized (from Ce^{3+} to Ce^{4+}), it is often found enriched in Mn-rich crusts, resulting in a positive Ce anomaly (Ohta and Kawabe, 2001; Thiagarajan and Lee, 2004). Measurements of urban air in Madrid, Spain (0.76 ng m^{-3} Ce) revealed positive Ce anomalies ($Ce^* = 1.27$) (Moreno et al., 2013). Cerium is thought to be enriched in air due to vehicle emissions from catalytic converters (Moreno et al., 2013) and from cerium oxide-based diesel fuel additives (Park et al., 2008). However, if Ce is abundant in PM in its oxidized form (CeO_2), it is insoluble and will not become enriched by scavenging processes of Mn oxyhydroxides. The lack of a positive Ce anomaly in the crusts at the minster might thus be due to the rapid accumulation of the crusts in addition to the PM containing primarily insoluble Ce^{4+}.

Element maps of Mn obtained by STXM—NEXAFS measurements (Fig. 8a) show that the black crust has an additional coating of a carbon- and nitrogen-rich substance, presumably organic matter (Fig. 8b). Underneath the Mn-coating, two additional spots of C-rich material can be observed (Fig. 8b). The carbon underneath the crust has no direct contact to the Mn crust, and the spots are too small to possibly be bacterial cells (< < 1 μm). Cluster analysis of the STXM-NEXAFS energy stack scans was conducted. It was used to determine if the carbon material underneath the crusts is similar to the organic layer on top of the crust. The results show two similar C-rich clusters (Fig. 8c, d) with sharp and strong absorption edges of several different functional groups (Fig. 8e, f). These two clusters reveal that the carbon from underneath the Mn-rich crust has the same functional groups as the carbon on top of the crust (Fig. 8d, f) and the two C-rich spots could thus have been introduced into the Mn-layer through an open cavity system. Resonance peaks of carbon were found at 284.7 eV (quinones), 285.4 eV (aromatic carbon), 286.3 eV (aryl, vinyl-keto), 287.65 eV (aliphatic group), and 288.85 (carboxyl group), showing the broad range of different moieties within the material (Cody et al., 2008; Lehmann et al., 2005). For comparison, a NEXAFS spectrum of Bacillus subtilis is also plotted in Fig. 9, to illustrate that the spectrum does not confirm the presence of bacteria. Additionally plotted are soot (Hopkins et al., 2007; Obst et al., 2011) and polycyclic aromatic hydrocarbon (Braun et al., 2007; Solomon et al., 2009) spectra for comparison, which indicate that the carbon fraction of sample J12SC is a mixture of

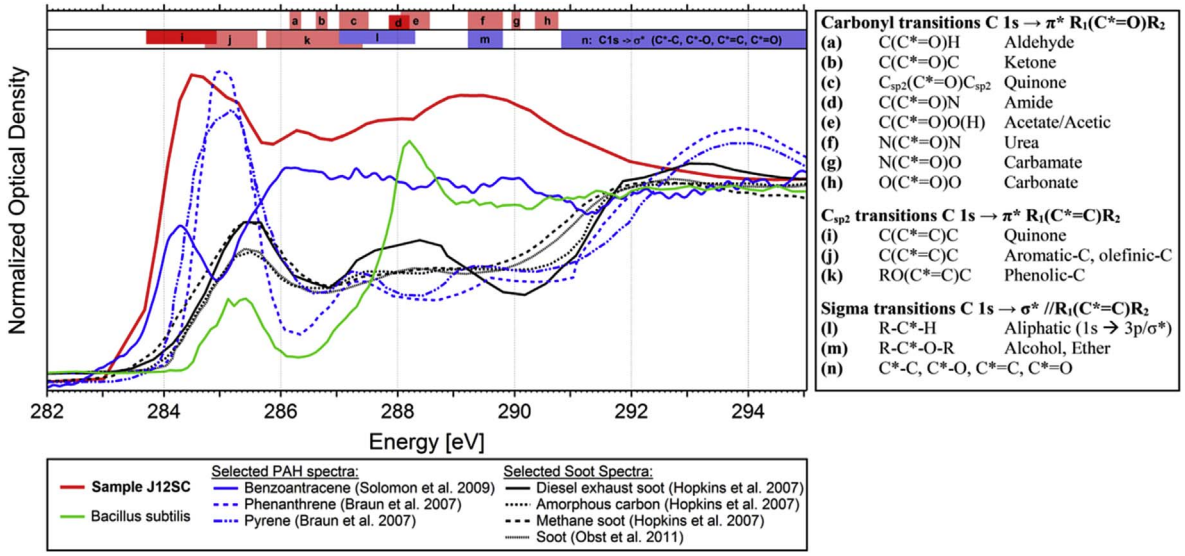

Fig. 9. Scanning transmission X-ray microscopy-NEXAFS spectra of sample J12SC. The spectrum of the sample (red) corresponds well with a mixture of soot and PAH, based on literature data. The bacillus subtilis spectrum (green), measured in addition, does not agree with the spectrum obtained from the minster's wall. (For interpretation of the references to colour in this figure legend, the reader is referred to the web version of this article.)

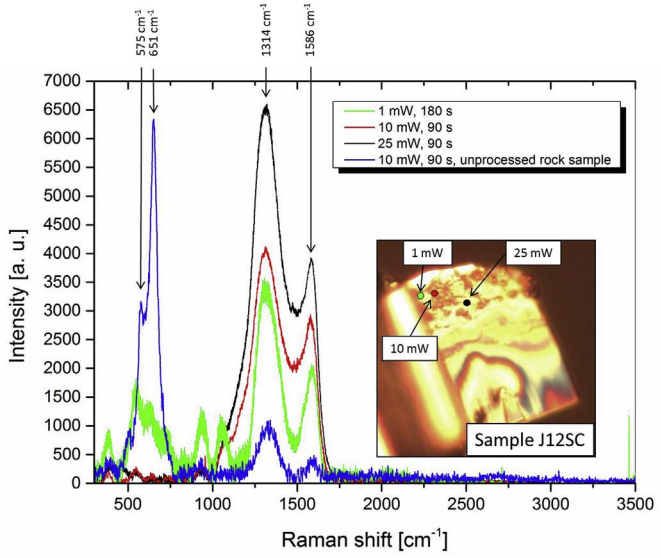

Fig. 10. Raman spectra of sample J12SC measured with different power settings. The power was increased from 1 mW up to 25 mW. To confirm that the spectrum was not produced by degradation of the thin sample (thickness of 100–200 nm), a spectrum of the unprocessed rock surface was taken. This spectrum shows the same soot-like bands (1314 cm^{-1}, 1586 cm^{-1}), as well as additional dominating birnessite bands (575 cm^{-1}, 651 cm^{-1}) of the Mn-crust underneath the C-rich crust.

soot and different polyaromatic compounds (Fig. 9). The presence of bacteria or fungi that might be involved in Mn deposition can thus be excluded. Raman spectroscopic measurements of the material also indicate the substance to be a soot-like material (bands at 1314 cm^{-1} and 1586 cm^{-1}), and also exclude the abundance of bacteria or fungi (Fig. 10). The C-rich crust on the FIB-prepared sample J12SC shows distinct soot bands (Patel et al., 2012; Sadezky et al., 2005; Sahoo and Kandasubramanian, 2014), which increase with increasing power settings. The additionally measured unprocessed sample J12SC shows a mixture of soot and birnessite bands (Freitas et al., 2013; Gui et al., 2015; Julien and Massot, 2002). Birnessite is a Mn oxyhydroxide phase that is typical of terrestrial Mn-rich crusts, and thus not unexpected in this context. The mixture of both materials results from the measurements having been made perpendicular to the surface, probing into both the C-rich and Mn-rich layer. Hence, we conclude that this carbon is not directly involved in the crusts genesis, and that no indication for a biogenic genesis was found. Whether the Mn-rich layer is still growing under the thick carbon-rich crust cannot be determined.

3.6. Renaissance-Vorhalle

At the Freiburger Münster, manganese-rich (> 150 μg cm^{-2}) patches are only found up to a height of about 7 m, with decreasing amounts at higher elevations. This makes the Renaissance-Vorhalle an exception, with exceptionally high Mn mass fractions at a height of about 7.7 m. One difference between the Renaissance-Vorhalle and the rest of the Münster is that it was treated with a hydrophobic, diffusion-open silicon resin paint (Firma Remmers) during its restoration in 2003. This paint permits diffusion of water through the paint to the air/paint surface, where it can slowly evaporate. When this paint develops fissures or cracks, water can intrude between the paint and the sandstone. The approximate locations of fissures and cracks can be detected by observing the rocks after a rain event (Fig. 11). The rock surfaces under and around these cracks stay wet, while other surfaces dry quickly, due to the hydrophobic character of this paint. It can be observed that the Mn-rich crusts, as well as organic growth, develop preferentially on top of these wet surfaces (Fig. 11). Since the paint has a pH value of about 8–9, Mn^{2+}, which is mobile and stable under slightly acidic conditions such as in rain within urban areas, might start precipitating under oxic conditions. If surfaces that are supplied with water (by diffusion of rainwater through the paint), have an alkaline pH value, and get an additional supply of Mn^{2+} from atmospheric aerosols, the precipitation of Mn oxyhydroxide crusts could start. The steady supply of small amounts of water over a long time period through a diffusion-open paint could explain the faster accumulation of the crusts even at these high elevations. Since the water underneath the paint moves around structures protruding out on vertical surfaces, these structures remain initially uncovered by the crusts (Fig. 12a) until the crust is too thick elsewhere to allow diffusion. As a consequence, the paint covering the protruding structures is subsequently activated and crusts can start to develop on these surfaces as well (Fig. 12b). Crusts can continue growing by autocatalysis, even if the water supply by the paint is constrained due to sealing by a crust, until the crusted areas start to exfoliate from the rock together with the paint itself (Fig. 12c). Crusts with 1200 μg cm^{-2} Mn were measured on top of the silicon resin,

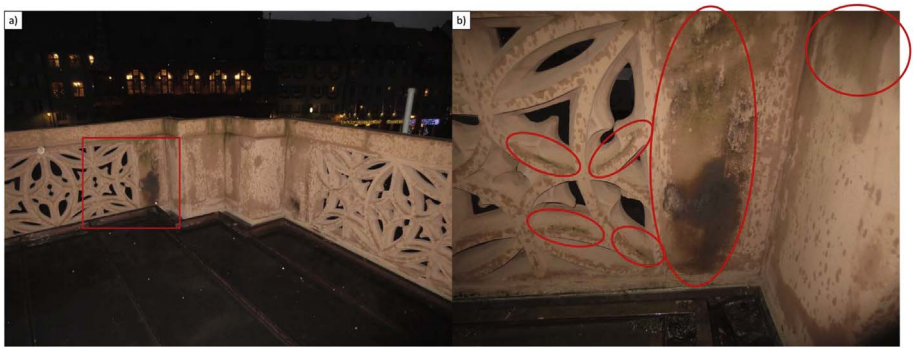

Fig. 11. The Renaissance-Vorhalle during a rain-event (a) and a close-up view of a Mn-rich crust (b). Black crusts and biogenic material develop at surfaces which get wet and remain wet in spite of the hydrophobic silicon resin paint. One can presume that the paint is too thin on these surfaces, or that fissures or cracks allow water to intrude between the paint and the rock. (For interpretation of the references to colour in this figure legend, the reader is referred to the web version of this article.)

which had grown in the period between 2003 and 2015. This suggests an accumulation rate of about 100 μg cm^{-2} a^{-1}. Such high Mn accumulation rates are not explainable by usual dry or wet deposition and condensation, being about 50 times higher than expected. Even a faster and more frequent precipitation, as described above, does not satisfactorily solve the question about the Mn source for this high accumulation rate, and we can offer no explanation for the mechanism producing these extremely fast-growing crusts.

3.7. Schöpfungsportal

Of interest is also the Schöpfungsportal (Fig. 13) because of an existing photographic documentation spanning the last 100 years (Fig. 13). One black patch (lower yellow circle on the left side of the Portal, Fig. 13g) developed in a time period of ≤100 years, between about 1913 and 2007. Two additional black crusts at the Schöpfungsportal (upper yellow circles on the left side of the Portal, Fig. 13e and f) developed within no more than four years (between 2007 and 2011). This observation indicates that the development of these patches is very fast as well. An explanation for the two new patches could be the treatment of the Schöpfungsportal between 2005 and 2007 during the restoration. In contrast to the paint used for the Renaissance-Vorhalle, which is hydrophobic and diffusion-open, the coating at the Schöpfungsportal was used to seal pore systems and is intended to be closed to water diffusion. A silicic acid ester ($Si(OR)_4$) was applied to the surface to preserve it ($Si(OC_2H_5)_4 + 4\ H_2O \rightarrow SiO_2 \cdot n\ H_2O + 4\ C_2H_5OH$). However, to allow the reaction from the intermediate -SiOH-HOSi- structures to an amorphous silica gel consisting of SiO_2 and water to proceed fast enough, an alkaline catalyst is added to initiate the hydrolysis. When the vapors produced by the reactions exit the system, the volume of the paint changes. At areas where the coating is exceptionally thick, a system of fissures evolves. This is the area where rainwater can enter and remain for a longer time period. This Mn-enriched rainwater in combination with the alkaline catalyst can result in the oxidation of Mn by alkalization of the system and precipitation of Mn oxyhydroxides. The final product can be the rapid development of the two new patches observed at the Schöpfungsportal.

4. Conclusion

Most of the patches found at the facade of the Freiburger Münster at a height of > 7 m are Mn-free. They seem to originate most likely from soot or biopigments of black fungi (Fig. 6), rather than from Mn accumulation. In contrast, almost all black patches at heights up to 7 m revealed high mass fractions of Mn. This height limitation corresponds to the heights up to which vehicle emissions and movements dominate the pollutant levels, and to the flow and turbulence of air masses. The enrichment within the patches with high Mn amounts is unlikely to originate from the sandstone building blocks, and atmospheric deposition of Mn is favored as the possible source of Mn. Vehicle emissions with their high Mn, Pb, Zn, and Ba mass fractions are very likely the metal sources for the airborne particles. This is in agreement with the high amounts of the trace elements Pb, Ba, and Zn found within the crusts.

We used a portable XRF to measure Mn surface densities in μg cm^{-2}. Thus, an approximate growth rate can be calculated for the

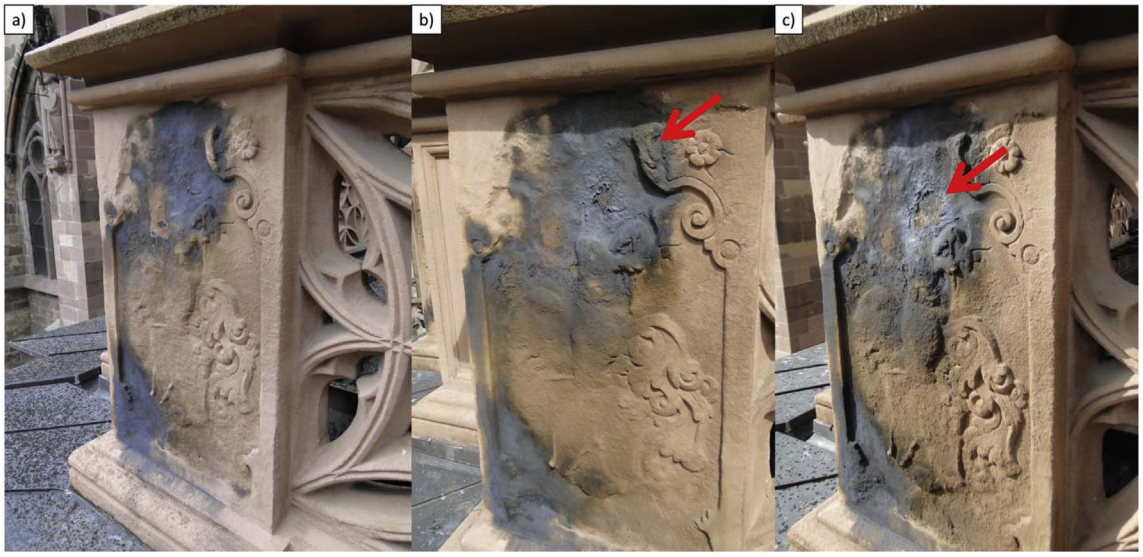

Fig. 12. : Stone carving at the Renaissance-Vorhalle photographically documented over a time period of three years, a) 2012, b) 2015, c) 2016. The crust develops rapidly with time, overgrowing higher elevated structures (marked in b). When the crust becomes too thick, exfoliation follows (marked in c). (Image credits: Freiburger Münsterbauverein).

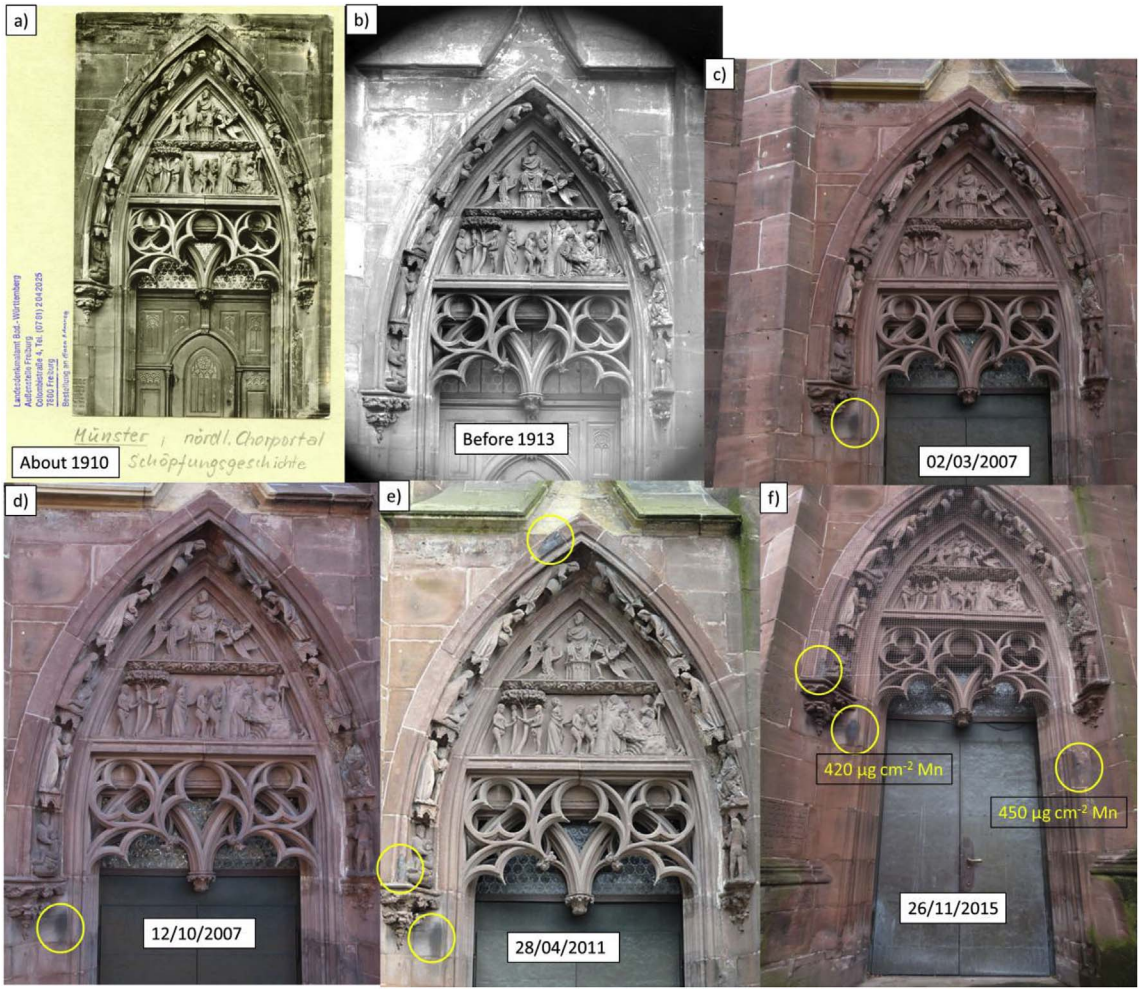

Fig. 13. The Schöpfungsportal of the Freiburger Münster, photographed over a period of more than 100 years: The development of black crusts can be monitored. Black crusts are marked by yellow circles. In Fig. 13 f, measured Mn surface densities are also shown. (Image credit Fig. 13 a: Landesamt für Denkmalpflege im RP Stuttgart; image credit Fig. 13 b: Münsterbauverein Freiburg; image credits Fig. 13 c and d: J. Quatmann, restorer; image credits Fig. 13 e: Wikicommons, user: Daderot, Lizense: Creative Commons CC0 1.0 Universal Public Domain Dedication). (For interpretation of the references to colour in this figure legend, the reader is referred to the web version of this article.)

crusts on the minster. Calculations strongly indicate wet deposition as the major Mn deposition mechanism, in combination with dry deposition, condensed water, and clay mineral interaction. Manganese from vehicle sources has a leachable fraction of about 90%, allowing the high Mn enrichment found within the crusts. The oxidation from mobile Mn^{2+} to immobile Mn^{4+} appears to happen abiogenically, via pH shifts from acidic rain to alkaline conditions caused by the alkali and earth alkaline metal containing minerals and clay minerals in sandstones. Biogenic oxidation can be excluded as a factor in the Mn precipitation at the Freiburger Münster. No evidence for organisms was found, neither by light microscopy nor in the course of the search for functional groups and remains of bacterial structures by X-ray microspectroscopy. Raman spectroscopic investigations support the finding of a soot-like material as the only form of organics present in the crust, and confirm the presence of the mineral birnessite as the predominant Mn-bearing mineral.

The element composition of the minster's crusts is similar to that of common rock varnishes, however, the source materials and formation mechanism seem to differ. While rock varnish has a major contribution to its formation by deposition and leaching of mineral dust, the minster's crusts seem to be dominated by anthropogenic emissions and, if at all, only marginally influenced by natural dust minerals.

On the Schöpfungsportal and the Renaissance-Vorhalle, the crusts are especially thick. Since the crusts on the Renaissance-Vorhalle grew on top of a resin applied in 2003, an accumulation rate of more than 100 µg cm^{-2} a^{-1} can be estimated, assuming a uniform growth from 2003 until 2015. Alkaline additives to coloring and pore-space-sealing agents might have contributed to this phenomenon, but we cannot satisfactorily explain the extremely high Mn growth rates on this part of the building.

In conclusion, black patches on building facades, usually interpreted as soot or biopigments until now, seem to be often Mn-rich deposits. Three different kinds of Mn-rich patches were observed on the Freiburger Münster: 1) thin Mn-rich crusts on vertical surfaces, 2) relatively thick crusts, which grew rapidly, on the Schöpfungsportal, and 3) especially fast growing and thick crusts, which show exfoliation due to the underlying silicon resin layer, at the Renaissance-Vorhalle. Black, Mn-rich crusts have been found on several buildings tested for such patches at locations distributed worldwide. This indicates that the phenomenon is more common than expected until recently, and further investigations are of scientific interest as well as of great importance for monument conservation and restoration. They are especially needed to prevent restorers to undertake decisions planned to stop the crusts' growth, which, on the contrary, accelerate the growth rates and damage the building facades of objects of historical interest, as it was observed at the Freiburger Münster.

Acknowledgments

This work was supported by the Max Planck Graduate Center with

the Johannes Gutenberg University Mainz (MPGC) and the Max Planck Society. We want to thank Maik Biegler for the sample preparation for the LA-ICP-MS measurements and the Münsterbauverein Freiburg, Luzius Kürten, and Uwe Zäh for making it possible to conduct this research. We would like to thank Petya Yordanova for assistance during microscopy and R. Livingston for bringing up the idea to investigate urban varnish. Furthermore, we would like to thank the Münsterbauverein Freiburg, Johanna Quatmann, and the Landesamt fuer Denkmalpflege im Regierungspräsidium Stuttgart for providing images. We thank J. J. Schauer and M. M. Shafer for sharing their unpublished data on Mn in European aerosols. This work was supported by the Max Planck Graduate Center with the Johannes Gutenberg University Mainz (MPGC), the Max Planck Society, and King Saud University. The ALS is supported by the Director, Office of Science, Office of Basic Energy Sciences, of the US Department of Energy under Contract DE-AC02-05CH11231. We thank the Helmholtz-Zentrum Berlin for the allocation of the synchrotron radiation beamtime at BESSY II.

Appendix

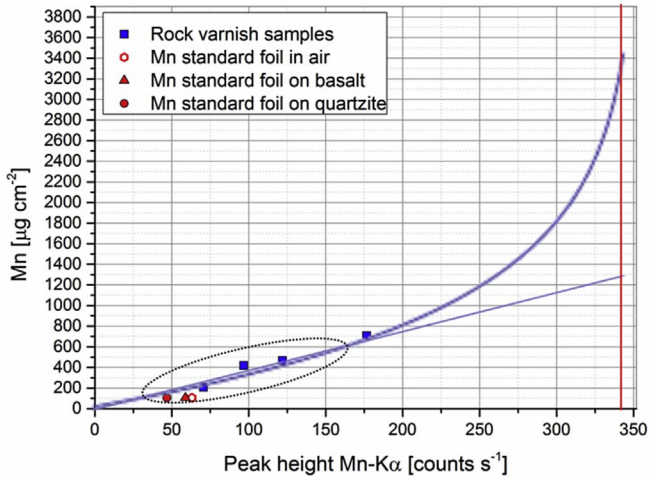

Figure A. Two different calibration curves to recalculate the Mn-Kα peak height into a surface density, a logarithmic fit and a linear fit. For the range where most of the measurements as well as the calibration values are located (circled area), the calculated surface density does not change significantly using the different fit parameters. The logarithmic equation would be D= (ln(A/(A-I)))/B, where I is the Intensity [cps], D is the surface density [µg cm^{-2}], and A and B are fit parameters.

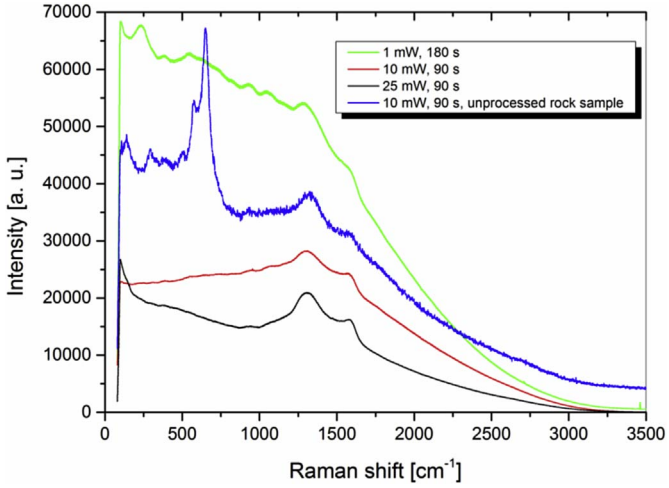

Figure B. Raw spectra of all Raman measurements plotted in Fig. 10. For the baseline correction, the spectra from 80 to 300 cm^{-1} were cut in order to allow a reasonable background subtraction.

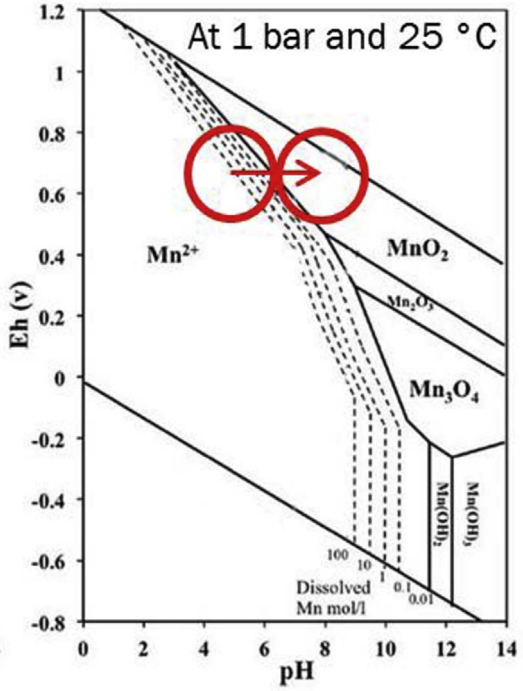

Figure C. Pourbaix or pH-E_h diagram of Mn-H_2O at 1 bar and 25 °C, modified from Goldsmith et al. (2014). The circle to the left represents the conditions one would expect in rainwater, where Mn is available as mobile Mn^{2+}. The shift to a higher pH value due to the uptake of protons by clay minerals or the exposition to alkali and alkaline earth metal containing minerals is represented by the arrow. The final range where the solution might remain is shown by the right circle, a field in which Mn is stable as immobile Mn^{4+} and might precipitate, especially in the presence of catalysts, as Mn oxyhydroxide.

References

Barrea, R., Bengio, S., Derosa, P., Mainardi, R., 1998. Absolute mass thickness determination of thin samples by X-ray fluorescence analysis. Nucl. Instrum. Methods Phys. Res. Sect. B Beam Interact. Mater. Atoms 143, 561–568.

Birmili, W., Allen, A.G., Bary, F., Harrison, R.M., 2006. Trace metal concentrations and water solubility in size-fractionated atmospheric particles and influence of road traffic. Environ. Sci. Technol. 40, 1144–1153.

Blau, P.J., 2001. Compositions, Functions, and Testing of Friction Brake Materials and Their Additives. Oak Ridge National Lab., TN (US).

Bonazza, A., Brimblecombe, P., Grossi, C.M., Sabbioni, C., 2007a. Carbon in black crusts from the tower of London. Environ. Sci. Technol. 41, 4199–4204.

Bonazza, A., Sabbioni, C., Ghedini, N., 2005. Quantitative data on carbon fractions in interpretation of black crusts and soiling on European built heritage. Atmos. Environ. 39, 2607–2618.

Bonazza, A., Sabbioni, C., Ghedini, N., Hermosin, B., Jurado, V., Gonzalez, J.M., Saiz-Jimenez, C., 2007b. Did smoke from the Kuwait oil well fires affect Iranian archaeological heritage? Environ. Sci. Technol. 41, 2378–2386.

Braun, A., Mun, B.S., Huggins, F.E., Huffman, G.P., 2007. Carbon speciation of diesel exhaust and urban particulate matter NIST standard reference materials with C (1s) NEXAFS spectroscopy. Environ. Sci. Technol. 41, 173–178.

Breuer, B., Bill, K.H., 2006. Bremsenhandbuch: Grundlagen, Komponenten, Systeme, Fahrdynamik. Springer-Verlag.

Brimblecombe, P., Grossi, C.M., 2009. Millennium-long damage to building materials in London. Sci. Total Environ. 407, 1354–1361.

Brookins, D.G., 2012. Eh-pH Diagrams for Geochemistry. Springer Science & Business Media.

Cadle, S.H., Mulawa, P.A., Ball, J., Donase, C., Weibel, A., Sagebiel, J.C., Knapp, K.T., Snow, R., 1997. Particulate emission rates from in-use high-emitting vehicles recruited in Orange County, California. Environ. Sci. Technol. 31, 3405–3412.

Cody, G.D., Ade, H., Alexander, M.D., Araki, T., Butterworth, A., Fleckenstein, H., Flynn, G., Gilles, M.K., Jacobsen, C., Kilcoyne, A., 2008. Quantitative organic and light-element analysis of comet 81P/Wild 2 particles using C-, N-, and O-μ-XANES. Meteorit. Planet. Sci. 43, 353–365.

Cohen, J., 1992. A power primer. Psychol. Bull. 112, 155.

Conko, K.M., Rice, K.C., Kennedy, M.M., 2004. Atmospheric wet deposition of trace elements to a suburban environment, Reston, Virginia, USA. Atmos. Environ. 38, 4025–4033.

De Oliveira, B.P., De la Rosa, J., Miller, A., Sáiz-Jiménez, C., Gómez-Bolea, A., Braga, M.S., Dionísio, A., 2011. An integrated approach to assess the origins of black films on a granite monument. Environ. Earth Sci. 63, 1677–1690.

DePaul, F., Sheih, C., 1985. A tracer study of dispersion in an urban street canyon. Atmos. Environ. 1967 (19), 555–559.

Duvdevani, S., 1949. Dew observations and their significance—new methods in dew estimation. Proc. U. N. Sci. Conf. Conserv. Util. Resour. 45–47.

Duvdevani, S., 1953. Dew Gradients in Relation to Climate, Soil and Topography. Desert Research Symposium, Jerusalem, pp. 136–152.

Espinosa, A.J.F., Rodríguez, M.T., de la Rosa, F.J.B., Sánchez, J.C.J., 2002. A chemical speciation of trace metals for fine urban particles. Atmos. Environ. 36, 773–780.

Everett, L., Band, T., Burman, P., Butlin, R., Cooke, M., Cooke, R., 1988. The Effects of Acid Deposition on Buildings and Building Materials in the United Kingdom. Building Effects Review Group. Department of the Environment.

Follath, R., Schmidt, J.S., Weigand, M., Fauth, K., 2010. The X-ray microscopy beamline UE46-PGM2 at BESSY. Sri 2009: The 10th International Conference on Synchrotron Radiation Instrumentation. Eds: R. Garrett, I. Gentle, K. Nugent, S. Wilkins, 323-326.

Freitas, R.M., Perilli, T.A., Ladeira, A.C.Q., 2013. Oxidative precipitation of manganese from acid mine drainage by potassium permanganate. J. Chem. 2013.

Frierdich, A.J., Hasenmueller, E.A., Catalano, J.G., 2011. Composition and structure of nanocrystalline Fe and Mn oxide cave deposits: implications for trace element mobility in karst systems. Chem. Geol. 284, 82–96.

Garg, B.D., Cadle, S.H., Mulawa, P.A., Groblicki, P.J., Laroo, C., Parr, G.A., 2000. Brake wear particulate matter emissions. Environ. Sci. Technol. 34, 4463–4469.

Goldsmith, Y., Stein, M., Enzel, Y., 2014. From dust to varnish: geochemical constraints on rock varnish formation in the Negev Desert, Israel. Geochimica Cosmochimica Acta 126, 97–111.

Gorbushina, A., Krumbein, W., Hamman, C., Panina, L., Soukharjevski, S., Wollenzien, U., 1993. Role of black fungi in color change and biodeterioration of antique marbles. Geomicrobiol. J. 11, 205–221.

Grissom, C.A., Vicenzi, E.P., Livingston, R.A., Aloiz, E., Little, N., Giaccai, J., Freedman, W., 2014. Manganese in black crusts on Seneca sandstone. Microsc. Microanal. 20, 2044–2045.

Grossi, C., Brimblecombe, P., 2002. The effect of atmospheric pollution on building materials. J. de Physique IV Proc. EDP Sci. 197–210.

Grossi, C., Brimblecombe, P., 2008. Past and future colouring patterns of historic stone buildings. Mater. Construcción 58, 143–160.

Grüner, F., Wölbert, O., Kürten, L., Riemann, J., 2011. Verschwärzung von Sandsteinoberflächen durch Eisen-/Manganoxide, neue Ergebnisse zu Ursache und restauratorischer Behandlung mittels Kompressen. Natursteinsanierung Stuttgart 2011. Neue Natursteinsanierungsergebnisse und messtechnische Erfassungen sowie Sanierungsbeispiele Conference, 7–21.

Guha, A., 1997. A unified Eulerian theory of turbulent deposition to smooth and rough surfaces. J. Aerosol Sci. 28, 1517–1537.

Gui, Z., Gillette, E., Duay, J., Hu, J., Kim, N., Lee, S.B., 2015. Co-electrodeposition of RuO 2–MnO 2 nanowires and the contribution of RuO 2 to the capacitance increase. Phys. Chem. Chem. Phys. 17, 15173–15180.

Hem, J.D., 1963. Chemical Equilibria and Rates of Manganese Oxidation. USGPO.

Hicks, B.B., 2005. A climatology of wet deposition scavenging ratios for the United States.

Atmos. Environ. 39, 1585–1596.
Hopkins, R.J., Tivanski, A.V., Marten, B.D., Gilles, M.K., 2007. Chemical bonding and structure of black carbon reference materials and individual carbonaceous atmospheric aerosols. J. Aerosol Sci. 38, 573–591.
Iijima, A., Sato, K., Yano, K., Kato, M., Kozawa, K., Furuta, N., 2008. Emission factor for antimony in brake abrasion dusts as one of the major atmospheric antimony sources. Environ. Sci. Technol. 42, 2937–2942.
Janssen, N.A., Van Mansom, D.F., Van Der Jagt, K., Harssema, H., Hoek, G., 1997. Mass concentration and elemental composition of airborne particulate matter at street and background locations. Atmos. Environ. 31, 1185–1193.
Jochum, K.P., Weis, U., Schwager, B., Stoll, B., Wilson, S.A., Haug, G.H., Andreae, M.O., Enzweiler, J., 2016. Reference values following ISO guidelines for frequently requested rock reference materials. Geostand. Geoanalytical Res. 40, 333–350.
Julien, C., Massot, M., 2002. Spectroscopic studies of the local structure in positive electrodes for lithium batteries. Phys. Chem. Chem. Phys. 4, 4226–4235.
Kilcoyne, A.L.D., Tyliszczak, T., Steele, W.F., Fakra, S., Hitchcock, P., Franck, K., Anderson, E., Harteneck, B., Rightor, E.G., Mitchell, G.E., Hitchcock, A.P., Yang, L., Warwick, T., Ade, H., 2003. Interferometer-controlled scanning transmission X-ray microscopes at the advanced light source. J. Synchrotron Radiat. 10, 125–136.
Lehmann, J., Liang, B., Solomon, D., Lerotic, M., Luizão, F., Kinyangi, J., Schäfer, T., Wirick, S., Jacobsen, C., 2005. Near-edge X-ray absorption fine structure (NEXAFS) spectroscopy for mapping nano-scale distribution of organic carbon forms in soil: application to black carbon particles. Glob. Biogeochem. Cycles 19.
Livingston, R., Grissom, C., Vicenzi, E., Weldon-Yochim, Z., Little, N., Douglas, J., Fowler, A., Santelli, C., Macholdt, D., Ortiz-Montalvo, D., 2016. Investigation of urban rock varnish on the sandstone of the Smithsonian Castle. Sci. Art A Future Stone 399.
Macholdt, D., Jochum, K., Pöhlker, C., Arangio, A., Förster, J.-D., Stoll, B., Weis, U., Weber, B., Müller, M., Kappl, M., 2017. Characterization and differentiation of rock varnish types from different environments by microanalytical techniques. Chem. Geol. 459, 91–118.
Mann, H.B., Whitney, D.R., 1947. On a test of whether one of two random variables is stochastically larger than the other. Ann. Math. Stat. 50–60.
Martin, S.T., 2005. Precipitation and dissolution of iron and manganese oxides. Environ. Catal. 61–81.
Miller, A., Dionísio, A., Braga, M.S., Hernández-Mariné, M., Afonso, M., Muralha, V., Herrera, L., Raabe, J., Fernandez-Cortes, A., Cuezva, S., 2012. Biogenic Mn oxide minerals coating in a subsurface granite environment. Chem. Geol. 322, 181–191.
Moffet, R.C., 2011. Scanning Transmission X-ray Microscopy: Applications in Atmospheric Aerosol Research. Lawrence Berkeley National Laboratory.
Moreno, T., Karanasiou, A., Amato, F., Lucarelli, F., Nava, S., Calzolai, G., Chiari, M., Coz, E., Artíñano, B., Lumbreras, J., 2013. Daily and hourly sourcing of metallic and mineral dust in urban air contaminated by traffic and coal-burning emissions. Atmos. Environ. 68, 33–44.
Newby, P., Mansfield, T., Hamilton, R., 1991. Sources and economic implications of building soiling in urban areas. Sci. total Environ. 100, 347–365.
Nriagu, J.O., 1990. The rise and fall of leaded gasoline. Sci. total Environ. 92, 13–28.
Obst, M., Grathwohl, P., Kappler, A., Eibl, O., Peranio, N., Gocht, T., 2011. Quantitative high-resolution mapping of phenanthrene sorption to black carbon particles. Environ. Sci. Technol. 45, 7314–7322.
Ohta, A., Kawabe, I., 2001. REE(III) adsorption onto Mn dioxide (delta-MnO2) and Fe oxyhydroxide: Ce(III) oxidation by delta-MnO2. Geochim. Cosmochim. Acta 65, 695–703.
Okkenhaug, G., Almås, Å., Morin, N., Hale, S., Arp, H., 2015. The presence and leachability of antimony in different wastes and waste handling facilities in Norway. Environ. Sci. Process. Imp. 17, 1880–1891.
Oudijk, G., 2010. The rise and fall of organometallic additives in automotive gasoline. Environ. Forensics 11, 17–49.
Park, B., Donaldson, K., Duffin, R., Tran, L., Kelly, F., Mudway, I., Morin, J.-P., Guest, R., Jenkinson, P., Samaras, Z., 2008. Hazard and risk assessment of a nanoparticulate cerium oxide-based diesel fuel additive—a case study. Inhal. Toxicol. 20, 547–566.
Patel, M., Ricardo, C.L.A., Scardi, P., Aswath, P.B., 2012. Morphology, structure and chemistry of extracted diesel soot—Part I: transmission electron microscopy, Raman spectroscopy, X-ray photoelectron spectroscopy and synchrotron X-ray diffraction study. Tribol. Int. 52, 29–39.
Pesava, P., Aksu, R., Toprak, S., Horvath, H., Seidl, S., 1999. Dry deposition of particles to building surfaces and soiling. Sci. total Environ. 235, 25–35.
Pio, C.A., Ramos, M.M., Duarte, A.C., 1998. Atmospheric aerosol and soiling of external surfaces in an urban environment. Atmos. Environ. 32, 1979–1989.
Pöhlker, C., Wiedemann, K.T., Sinha, B., Shiraiwa, M., Gunthe, S.S., Smith, M., Su, H., Artaxo, P., Chen, Q., Cheng, Y., 2012. Biogenic potassium salt particles as seeds for secondary organic aerosol in the Amazon. Science 337, 1075–1078.
Potter, R.M., Rossman, G.R., 1977. Desert varnish: the importance of clay minerals. Science 196, 1446–1448.
Qin, Y., Kot, S., 1993. Dispersion of vehicular emission in street canyons, guangzhou city, south China (PRC). Atmospheric environment. Part B. Urban Atmos. 27, 283–291.
Reddy, M., Perkins, H., 1974. Fixation of zinc by clay minerals. Soil Sci. Soc. Am. J. 38, 229–231.
Reneau, S.L., 1993. Manganese accumulation in rock-varnish on a desert piedmont, Mojave Desert, California, and application to evaluating varnish development. Quat. Res. 40, 309–317.
Robert, J.C., 1984. Ethyl: a History of the Corporation and the People Who Made it. University Press of Virginia.
Rogge, W.F., Hildemann, L.M., Mazurek, M.A., Cass, G.R., Simoneit, B.R., 1993. Sources of fine organic aerosol. 3. Road dust, tire debris, and organometallic brake lining dust: roads as sources and sinks. Environ. Sci. Technol. 27, 1892–1904.
Root, R.A., 2000. Lead loading of urban streets by motor vehicle wheel weights. Environ. Health Perspect. 108, 937.
Ruffolo, S.A., Comite, V., La Russa, M.F., Belfiore, C.M., Barca, D., Bonazza, A., Crisci, G.M., Pezzino, A., Sabbioni, C., 2015. An analysis of the black crusts from the Seville Cathedral: a challenge to deepen the understanding of the relationships among microstructure, microchemical features and pollution sources. Sci. Total Environ. 502, 157–166.
Sadezky, A., Muckenhuber, H., Grothe, H., Niessner, R., Pöschl, U., 2005. Raman microspectroscopy of soot and related carbonaceous materials: spectral analysis and structural information. Carbon 43, 1731–1742.
Sahoo, B.N., Kandasubramanian, B., 2014. Photoluminescent carbon soot particles derived from controlled combustion of camphor for superhydrophobic applications. RSC Adv. 4, 11331–11342.
Sáiz-Jiménez, C., Hermosin, B., 2004. Black crusts in the European built environment. Corros. Rev. 22, 381–393.
Saiz-Jimenez, C., Miller, A.Z., Martin-Sanchez, P.M., Hernandez-Marine, M., 2012. Uncovering the origin of the black stains in Lascaux Cave in France. Environ. Microbiol. 14, 3220–3231.
Sanders, P.G., Dalka, T., Xu, N., Maricq, M.M., Basch, R., 2002. Brake Dynamometer Measurement of Airborne Brake Wear Debris (SAE Technical Paper). .
Schauer, J.J., Lough, G.C., Shafer, M.M., Christensen, W.F., Arndt, M.F., DeMinter, J.T., Park, J.-S., 2006. Characterization of Metals Emitted from Motor Vehicles. Research report (Health Effects Institute), 1-76; discussion 77–88. .
Sehmel, G.A., 1980. Particle and gas dry deposition: a review. Atmos. Environ. 1967 (14), 983–1011.
Solomon, D., Lehmann, J., Kinyangi, J., Liang, B., Heymann, K., Dathe, L., Hanley, K., Wirick, S., Jacobsen, C., 2009. Carbon (1s) NEXAFS spectroscopy of biogeochemically relevant reference organic compounds. Soil Sci. Soc. Am. J. 73, 1817–1830.
Takeno, N., 2005. Atlas of eh-pH diagrams. Geol. Surv. Jpn. open file Rep. 419, 102.
Thiagarajan, N., Lee, C.T.A., 2004. Trace-element evidence for the origin of desert varnish by direct aqueous atmospheric deposition. Earth Planet. Sci. Lett. 224, 131–141.
Tsunazawa, Y., Yokoyama, T., Nishiyama, N., 2016. An experimental study on the rate and mechanism of capillary rise in sandstone. Prog. Earth Planet. Sci. 3, 1–10.
Uchida, E., Watanabe, R., Osawa, S., 2016. Precipitation of manganese oxides on the surface of construction materials in the Khmer temples, Cambodia. Herit. Sci. 4, 1.
Vallero, D., 2014. Fundamentals of Air Pollution. Academic press.
Vicenzi, E.P., Grissom, C.A., Livingston, R.A., Weldon-Yochim, Z., 2016. Rock Varnish on Architectural Stone: Microscopy and Analysis of Nanoscale Manganese Oxide Deposits on the Smithsonian Castle. Heritage Science, Washington, DC, pp. 4.
Viles, H.A., Gorbushina, A.A., 2003. Soiling and microbial colonisation on urban roadside limestone: a three year study in Oxford, England. Build. Environ. 38, 1217–1224.
Wallace, L., Slonecker, T., 1997. Ambient air concentrations of fine (PM25) manganese in US National Parks and in California and Canadian cities: the possible impact of adding MMT to unleaded gasoline. J. Air & Waste Manag. Assoc. 47, 642–652.
Weigand, M., 2014. Realization of a New Magnetic Scanning X-ray Microscope and Investigation of Landau Structures under Pulsed Field Excitation. Universität Stuttgart Stuttgart (und Cuvillier Verlag, Göttingen).
White, W.B., Vito, C., Scheetz, B.E., 2009. The mineralogy and trace element chemistry of black manganese oxide deposits from caves. J. Cave Karst Stud. 71, 136–143.
Young, T.M., Heeraman, D.A., Sirin, G., Ashbaugh, L.L., 2002. Resuspension of soil as a source of airborne lead near industrial facilities and highways. Environ. Sci. Technol. 36, 2484–2490.